Mainz Microtron MAMI

Collaboration A2: "Real Photons"
Spokesperson: A. Thomas

Proposal for an Experiment

**" Photoproduction of η-mesons off the neutron –
Part I: Polarization observables with circularly polarized photons (E, T, F)"**

Collaborators:

CrystalBall@MAMI collaboration

Spokespersons for the Experiment:
I. Jaegle, University of Basel, Basel, Switzerland
B. Krusche, University of Basel, Basel, Switzerland

Abstract of Physics:
We propose to measure η-photoproduction from the neutron in particular in the energy range around 1 GeV incident photon energy (corresponding to W≈1.675 GeV). Previous experiments have shown a clear structure in the excitation function in this energy region, which is not seen in the excitation function of the proton and has a width of only ≈30 MeV. So far, the nature of this structure is unknown, model dependent analyses of the energy and angular dependence have not lead to conclusive results. We therefore propose the measurement of polarization observables in this energy regime. For MAMI we aim at the measurement of the observables E (circularly polarized photon beam, longitudinally polarized target) and T, F (circularly polarized photon beam, transversely polarized target). The measurement of T and F will at the same time complement proposal 2009-04, which aims at a measurement of T and F for the proton with special emphasis on the $S_{11}(1535)$ region.

Abstract of Equipment:
We require the 4π electromagnetic calorimeter consisting of the Crystal Ball and TAPS detectors combined with the Glasgow photon tagger. The PID detector is needed for the separation of recoil protons and neutrons going into the Crystal Ball detector. The measurement of the GDH observable E requires a circularly polarized beam on a longitudinally polarized neutron (deuterated butanol target), the measurement of T and F can be simultaneously done with a circularly polarized beam on transversely polarized target.

MAMI–Specifications:

beam energy	1558 MeV
beam current	< 100nA
time structure	cw
polarization	circularly polarized photons

Experiment–Specifications:

experimental hall/beam	A2
detector	Glasgow-Tagger, Crystal Ball, TAPS, PID
target material	polarized deuterated butanol

Beam Time Request:

set–up/tests with beam	24 hours
data taking	700 hours circularly pol. beam on pol. deuteron target
	already approved with A-rating by the previous PAC
	700 hours circularly pol. beam on transversely pol. target

List of participating authors:

- **Institut für Physik, University of Basel, Switzerland**
  I. Jaegle, I. Keshelashvili, B. Krusche, Y. Maghrbi, F. Pheron, T. Rostomyan, D. Werthmüller

- **Institut für Experimentalphysik, University of Bochum, Germany**
  W. Meyer, G. Reicherz

- **Helmholtz–Institut für Strahlen- und Kernphysik, University of Bonn, Germany**
  R. Beck, A. Nikolaev

- **Massachusetts Institute of Technology , Cambridge, USA**
  A. Bernstein, W. Deconinck

- **JINR, Dubna, Russia**
  N. Borisov, A. Lazarev, A. Neganov, Yu.A. Usov

- **School of Physics, University of Edinburgh, UK**
  D. Branford, D.I. Glazier, T. Jude, M. Sikora, D.P. Watts

- **Petersburg Nuclear Physics Institute, Gatchina, Russia**
  V. Bekrenev, S. Kruglov, A. Koulbardis

- **Department of Physics and Astronomy, University of Glasgow, UK**
  J.R.M. Annand, D. Hamilton, D. Howdle, K. Livingston, J. Mancell, J.C. McGeorge, I.J.D. Mac-Gregor, E.F. McNicoll, R.O. Owens, J. Robinson, G. Rosner

- **Department of Astronomy and Physics, Saint Mary's University Halifax, Canada**
  A.J. Sarty

- **Kent State University, Kent, USA**
  D.M. Manley

- **University of California, Los Angeles, USA**
  B.M.K. Nefkens, S. Prakhov, A. Starostin, I.M. Suarez

- **MAX-lab, University of Lund, Sweden**
  L. Isaksson

- **Institut für Kernphysik, University of Mainz, Germany**
  P. Aguar-Bartolome, H.J. Arends, S. Bender, A. Denig, E.J. Downie, N. Frömmgen, E. Heid, O. Jahn, H. Ortega, M. Ostrick, B.Oussena, P.B. Otte, S. Schumann, A. Thomas, M. Unverzagt

- **Institut für Physik, University of Mainz, D**
  J.Krimmer, W.Heil

- **University of Massachusetts, Amherst, USA**
  P.Martel, R.Miskimen

- **Institute for Nuclear Research, Moscow, Russia**
  G. Gurevic, R. Kondratiev, V. Lisin, A. Polonski

- **Lebedev Physical Institute, Moscow, Russia**
  S.N. Cherepnya, L.V. Fil kov, V.L. Kashevarov

- **INFN Sezione di Pavia, Pavia, Italy**
  A. Braghieri, A. Mushkarenkov, P. Pedroni

- **Department of Physics, University of Regina, Canada**
  G.M. Huber

- **Mount Allison University, Sackville, Canada**
  D. Hornidge

- **Tomsk Polytechnic University, Tomsk, Russia**
  A. Fix

- **Physikalisches Institut, University of Tübingen, Germany**
  P. Grabmayr, T. Hehl, D.G. Middleton

- **George Washington University, Washington, USA**
  W. Briscoe, T. Morrison, B.Oussena, B. Taddesse, M. Taragin
- **Catholic University, Washington, USA**
  D. Sober
- **Rudjer Boskovic Institute, Zagreb, Croatia**
  M. Korolija, D. Mekterovic, S. Micanovic, I. Supek

Preface

The two proposals: Photoproduction of η-mesons off the neutron:

<div>

Part I: Polarization observables with circularly polarized photons (E, T, F)

Part II: Polarization observables with linearly polarized photons (Σ, G, H, P)

</div>

deal with the same physics. Therefore the introduction, motivation and discussion of the physics case (sections 1.1 -2) are identical in the two proposals. The proposals differ in the description of the experimental setups and beam requirements (subsection 2.1). The proposals are independently submitted since one part of the measurements is proposed for the MAMI C facility in Mainz and the other part is proposed for the ELSA facility in Bonn. Both proposals are updates of the previously approved proposals A2-10, ELSA-3 which in the meantime have only partly been worked of. The MAMI part of the proposal has also overlap with the proposal A2-4-09 which aims at the investigation of the observables T and F for η-production off the proton in the S_{11}-range. Both proposals have furthermore overlap with the measurement of the respective polarization observables for other reaction channels, e.g. with the GDH sum-rule off the neutron.

1 Photoproduction of η mesons off the neutron

1.1 Introduction and Motivation

The excitation spectrum of baryons is closely connected to the properties of QCD in the low-energy regime, where it cannot be treated in perturbative approaches. Lattice gauge calculations have provided results for the ground state properties and more recently also for some excited states (see e.g. Ref. [1]), but the prediction of the excitation spectrum is still out of reach even for the most powerful computer systems. The connection between experimental observations and QCD is mostly done with QCD inspired quark models. However, the basis of these models is still not well anchored. There is neither consent about the effective degrees of freedom nor about the residual quark - quark interactions (see e.g. Ref. [2] for a recent overview). Furthermore, a comparison of the experimentally known excitation spectrum to model predictions reveals severe problems for all types of models. The ordering of some of the lowest lying states is not reproduced. In particular, the $N^\star$ $P_{11}(1440)$ ('Roper') resonance and the first excited Δ, the $P_{33}(1600)$, which in the quark model belong to the N=2 oscillator shell, appear well below the states from the N=1 shell. Furthermore, even the models with the fewest number of effective degrees of freedom predict many more states than have been observed. Since most states have been observed with elastic scattering of charged pions it is thus possible that the data base is biased for states that couple only weakly to πN. Therefore photon induced reactions, which nowadays can be investigated with comparable precision as hadron induced reactions, have moved into the focus. At the modern facilities (ELSA in Bonn, GRAAL in Grenoble, JLAB in Newport News, MAMI in Mainz and Spring8 in Osaka) these experiments have developed into two directions: measurements up to high excitation energies with the aim to identify at least some of the 'missing' states (see e.g. [3]) and precise investigations of the properties of known low lying nucleon resonances (see e.g. [4]).

Over the last few years the combination of linearly and circularly polarized photon beams with polarized targets at Jlab, ELSA and from 2010 on also at MAMI have added new powerful tools for the identification of contributions from resonances with different quantum numbers to meson photoproduction reactions. This will allow a much more efficient investigation of resonance properties since one may select for any resonance of interest the most sensitive combination of experimental observables.

Although experimental programs for the study of nucleon resonances off the proton via photoproduction of mesons are well developed, so far much less effort has gone into the investigation of the corresponding reactions on the neutron. Photoproduction of mesons off the neutron serves two different purposes. First, this is the only possibility to disentangle the isospin structure of the electromagnetic resonance excitations, which serves as one stringent test of baryon model predictions. Secondly, in some cases the electromagnetic coupling of resonances to the neutron ground state may be much stronger than in the proton case, so that certain resonances potentially can be studied in more detail on the neutron.

The investigation of photoproduction reactions off the neutron is of course complicated by the non-availability of free neutron targets, which requires the use of light nuclei as target materials. The deuteron with its low binding energy is clearly the best target choice for most measurements on the neutron. However, the measurement off bound neutrons does not only smear excitation functions and kinematical observables due to the momentum distribution of the nucleons, it also introduces additional uncertainties due to nuclear effects like final state interaction (FSI) or interference terms. The actual importance of such nuclear effects may be very different for different meson production reactions. Substantial effects have been found for example in the photoproduction of π^o mesons off the deuteron in the Δ-resonance region and in the second resonance region. In the first case the measured cross sections [5] could only be understood [6] when FSI (in particular NN FSI) was thoroughly treated in the models. The experimental results of inclusive π^o photoproduction in the second resonance region are even still not fully understood (see [4] for an overview). However, the situation is much more favorable for the photoproduction of η mesons, which is the topic of this proposal. This is demonstrated in fig. 1. The left hand side shows the influence of final state interaction on the threshold behavior of inclusive η-production of the deuteron calculated by Sibirtsev et al. [7] (other models give qualitatively similar results). Although FSI is large close to the kinematic threshold for η production of the deuteron, it is already completely negligible at energies larger than the threshold on the free proton (707 MeV). Even more suggestive is the comparison of free and quasi-free production of the proton in the right hand side of the figure. The cross section measured for the quasi-free reaction $\gamma d \to \eta p(n)$ by coincident
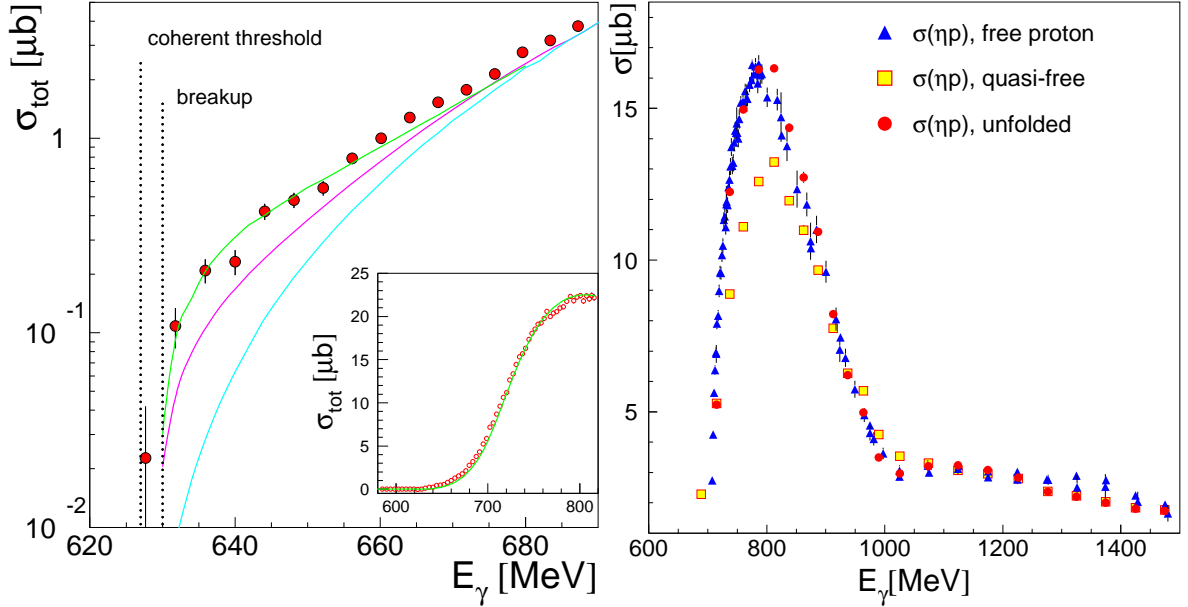
Figure 1: Left hand side: threshold behavior of the inclusive $\gamma d \to \eta X$ reaction compared to calculations PWIA (blue), with NN-FSI (magenta) and with full FSI (green) contributions [7]. Insert: data and most simple PWIA [8] over larger energy range. Right hand side: comparison of free and quasi-free data for η-production of the proton. Blue triangles: $\gamma p \to p\eta$, Squares: $\gamma d \to \eta p(n)$, red circles: $\gamma d \to \eta p(n)$ after correction for Fermi smearing (deuteron data from ELSA experiment [9]).

detection of the recoil proton [9] is reduced in the S_{11} peak due to Fermi smearing. However, since the free proton cross section is well known, one can calculate a correction for that from a comparison of the free cross section to the free cross section folded with the momentum distribution of the nucleons in the deuteron. After applying this correction to the quasi-free data, it agrees almost perfectly with the free proton data. Hence, for photoproduction off quasi-free protons no deuteron effects like FSI or re-scattering effects apart from Fermi smearing are observed.

Quasi-free and coherent photoproduction of η mesons off the deuteron, off ^{3}He, and off ^{4}He in the excitation range of the $S_{11}(1535)$ resonance has been studied during the last years in some detail [8, 10, 11, 12, 13, 14, 15] at different levels of sophistication. Again, the measured cross sections could be consistently understood in the framework of simple PWIA models, which took into account the Fermi motion of the bound nucleons. The comparison of the results from ^{4}He and the deuteron (see [4] for an overview) provide a stringent test of possible model dependent effects, since the influence of the different nuclear momentum distributions in the loosely bound deuteron and the strongly bound ^{4}He nucleus is severe. The total cross sections from ^{4}He and from the deuteron are almost equal at incident photon energies around 800 MeV, although twice the number of nucleons is involved in the He case. Nevertheless in both cases PWIA calculations with a 2/3 ratio of the free proton and neutron cross sections reproduces the data quite well. Typical cross section ratios from exclusive measurements with detection of recoil nucleons (see [4] for an overview) are summarized in fig. 2. Altogether, the results can be understood in simple plane wave approximations and FSI effects seem to play only a significant role in the vicinity of the production thresholds, which is not of interest for this proposal. The results, together with the measurements of coherent photoproduction of η mesons from light nuclei, have lead to a precise determination of the isospin structure of the excitation of the $S_{11}(1535)$ resonance [14]. Furthermore, it has specifically contributed to the discussion of the internal structure of this resonance. Kaiser et al. [16, 17] had suggested that this state does not correspond to a genuine three-quark structure but is more like a $K\Sigma$ nucleon-meson quasi-bound state. Their model reproduced the measured cross sections for $p(\gamma, p)\eta$ quite well, but it does not reproduce the neutron-proton cross section ratio (see fig.2).

At higher incident photon energy ($E_\gamma > 900$ MeV) models of η-photoproduction like the ETA-MAID model [19] predict a strong rise of the neutron - proton cross section ratio due to the contribution of
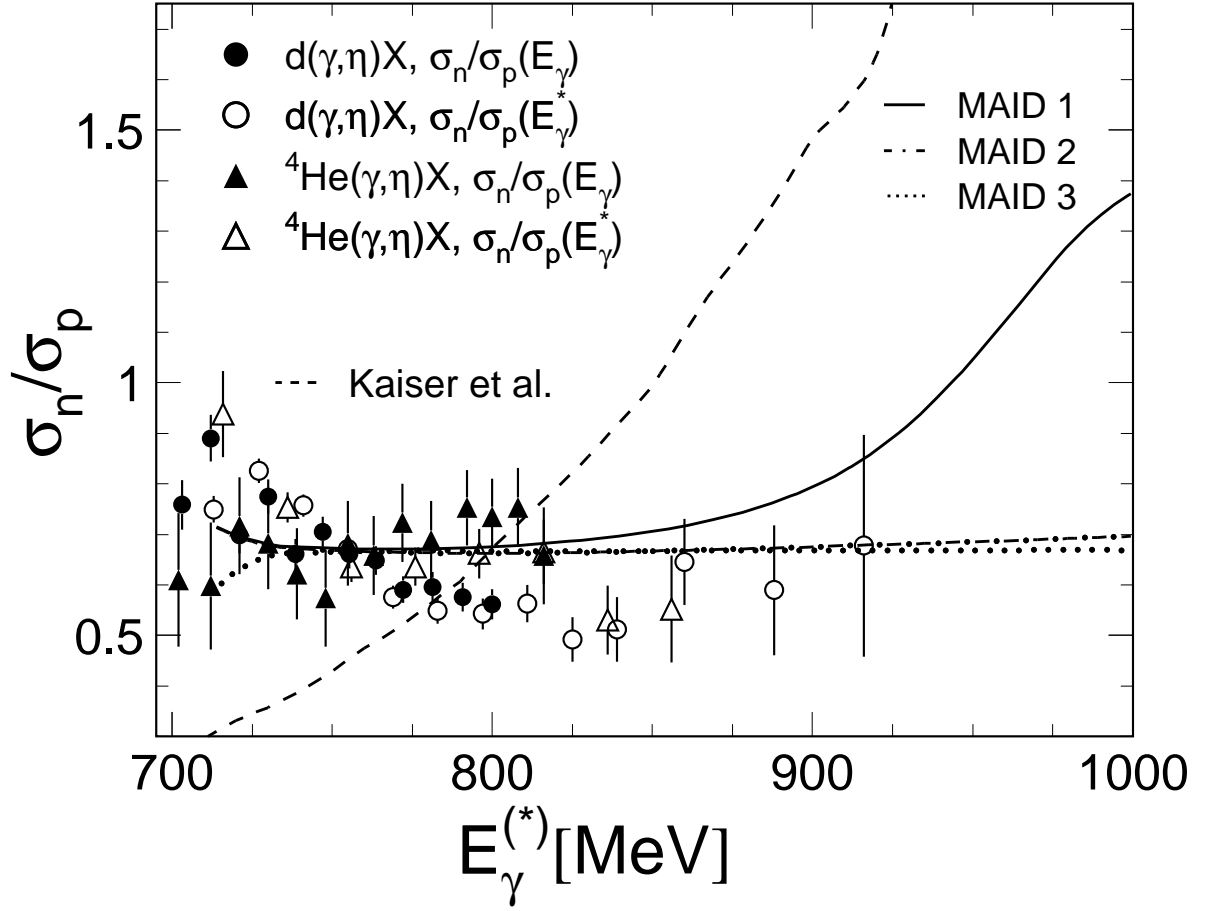
Figure 2: Measured ratio of the cross section of η photoproduction from the neutron and from the proton. Data are from obtained from deuteron and ^{4}He targets are from [14, 11]. Dashed curve: prediction from the $K\Sigma$ model of the $S_{11}(1535)$ (Kaiser et al. [16, 17]). The curves labeled MAID are the predictions from the MAID model [19] for the full model (MAID 1), the $S_{11}(1535)$-resonance, Born terms and vector meson exchange (MAID 2), and for the $S_{11}(1535)$ alone (MAID 3).

other nucleon resonances (see fig. 2). However, at photon energies around 1 GeV already the interpretation of the free proton data is so far controversial. It has been discussed in [18] that although the ETA-MAID model [19] and the Bonn-Gatchina (BoGa) analysis [20] describe differential cross sections and photon beam asymmetries equally well, the resonance contributions to the two models are quite different in this energy region. While for example the BoGa analysis finds a large contribution from the $P_{13}(1720)$ resonance, the results of the MAID-model are much more sensitive to the contributions of $P_{11}(1710)$ and $D_{13}(1520)$. Therefore also for the proton measurements of further polarization observables are very desirable and are under way at ELSA.

In the MAID model, the relative rise of he neutron cross section compared to the proton cross section which peaks at incident photon energies around 1 GeV, is mainly due to the excitation of the $D_{15}(1675)$ four star resonance. According to the review of particle properties (PDG) [21] this resonance has substantially larger photon couplings to the neutron than to the proton:

$$A_{1/2}^n = (-43 \pm 12) \cdot 10^3 \text{GeV}^{-1/2} \tag{1}$$

$$A_{3/2}^n = (-58 \pm 13) \cdot 10^3 \text{GeV}^{-1/2} \tag{2}$$

$$A_{1/2}^p = (+19 \pm 8) \cdot 10^3 \text{GeV}^{-1/2} \tag{3}$$

$$A_{3/2}^p = (+15 \pm 9) \cdot 10^3 \text{GeV}^{-1/2} \; . \tag{4}$$

In the framework of quark models there are predictions for a D_{15} resonance in this energy range with has a similar coupling pattern. A model which is based on single quark excitations from the nucleon
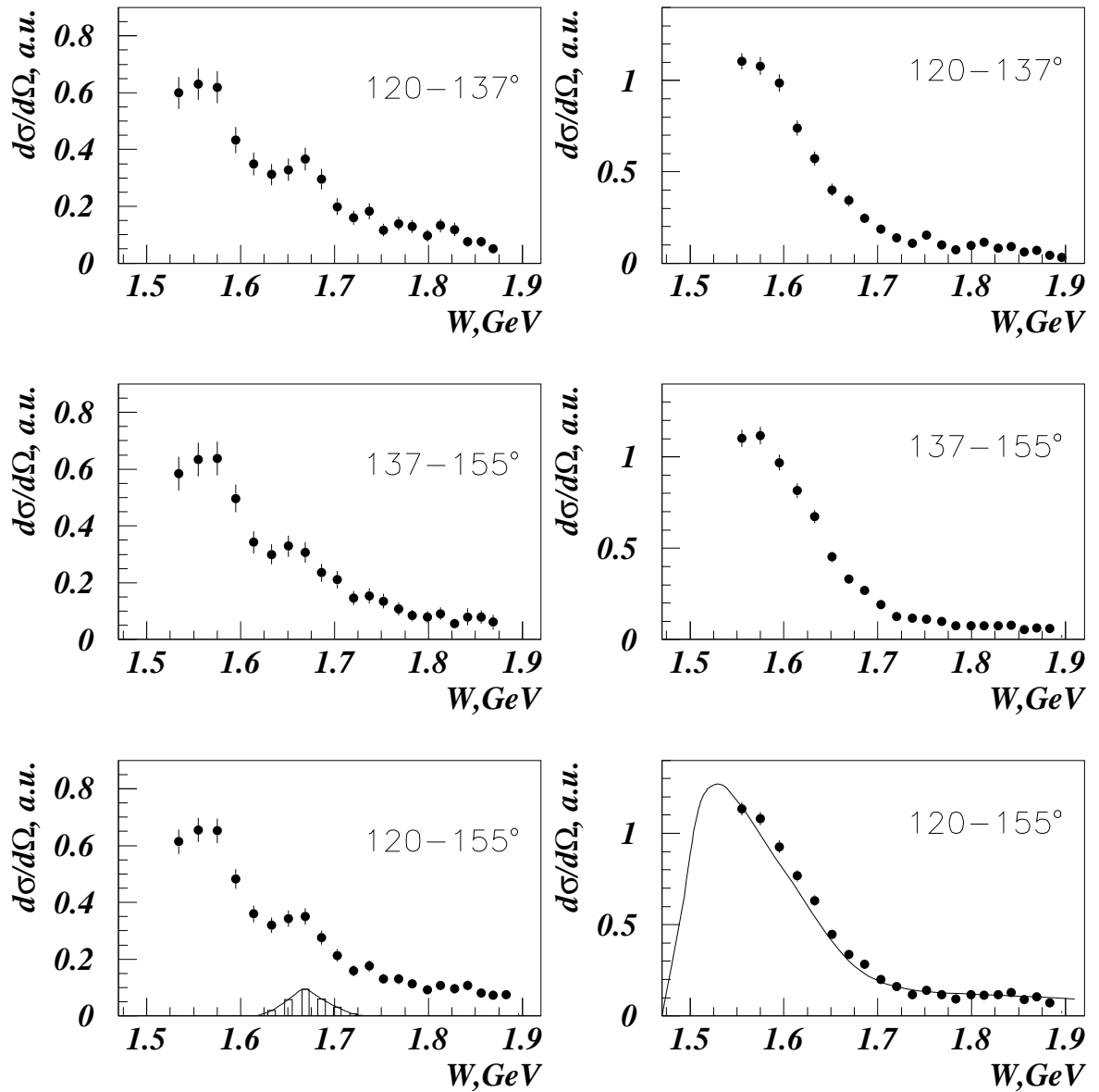
Figure 3: Preliminary results for quasi-free η-photoproduction off the proton (right hand side) and off the neutron (left hand side) from the GRAAL experiment [28] using a deuterium target. The solid line for the proton data shows the SAID [30] result for the free proton cross section.

ground state to the $[70,1^-]$ multiplet [22] predicts rather small photon couplings to the proton, but larger ones to the neutron. On the other hand, the decay branching ratio into the $N\eta$ final state of this resonance is estimated by the PDG in the range 0 - 1 %, i.e. so far no significant contribution to η photoproduction is established. Also an analysis of photoproduction off the proton, including the most recent η photoproduction data in this energy range [23], finds only a very small contribution of this resonance and a ratio of the helicity couplings ($A^p_{1/2}/A^p_{3/2} = 0.06 \pm 0.18$), which is in contradiction to the PDG value ($A^p_{1/2}/A^p_{3/2} = 0.93 \pm 0.18$). In summary, so far the contribution of this resonance to η photoproduction is not settled and only precise data for quasi-free photoproduction from the neutron can be expected to solve this question.

It is very interesting to note, that also in the framework of the chiral soliton model [24] a state is predicted in this energy range, with has much stronger photon couplings to the neutron than to the proton *and* a large decay branching ratio into $N\eta$. This state is the nucleon-like member of the predicted anti-decuplet of penta-quarks, which would be a P_{11} state. Exact SU(3)$_F$ would forbid the photo-excitation of the proton to the proton-like member of the anti-decuplet. But even after accounting for SU(3)$_F$ violation the chiral soliton model predicts [25] that the photo-excitation of this

state is suppressed on the proton and should mainly occur on the neutron. Kim et al. [26] have calculated the magnetic transitions moments for the anti-decuplet states and found a considerable enhancement for the excitation of the nucleon-like state on the neutron with respect to the proton. Also recent calculations [27] in a diquark picture of possible anti-decuplet states comes to a similar conclusion.

On the experimental side, the GRAAL collaboration [28, 29] has reported results for quasi-free η photoproduction off protons and off neutrons bound in the deuteron. The excitation functions for selected angular ranges are shown in fig. 3. The excitation functions of quasi-free η production measured in coincidence with recoil protons shows a smooth behavior and agrees as expected with the results for the free proton. However, on the neutron a relatively narrow structure is observed at incident photon energies around 1 GeV corresponding to $W \approx 1675$ MeV. From a simulation of a resonance structure, superimposed on a smooth background, Kutznetsov et al. [28], have extracted tentative values for the excitation energy and width of the visible structure as W=1675 MeV, Γ=40 MeV. Since the excitation function is smeared by the momentum distribution of the bound neutrons, the intrinsic width of the resonance-like structure must be even smaller. This would be clearly not in agreement with the parameters of the $D_{15}(1675)$ resonance discussed above which has an estimated width of 130 - 165 MeV [21]. It is therefore very urgent, to investigate quasi-free η photoproduction on the neutron in this energy regions in more detail. In particular the measurement of observables, which can pin down the quantum numbers of this structure is very desirable. It should be pointed out, that of course also the case of a conventional three quark state that is excited so dominantly on the neutron is of high interest for baryon spectroscopy.

1.2 Final results from the previous ELSA experiment

Triggered by the prediction of the MAID model of strong contributions from higher lying resonances to η photoproduction off the neutron, we had previously submitted a proposal to measure angular distributions for this reaction with the CBELSA/TAPS setup in Bonn. The experiment was successfully done in 2003 and the results (PhD thesis of I. Jaegle) have been published in Phys. Rev. Lett. It used the setup of the Crystal Barrel combined with the full TAPS detector configured as a forward wall. Eta-mesons were identified via their $\eta \rightarrow 3\pi^o \rightarrow 6\gamma$ decay. The $\eta \rightarrow 2\gamma$ decay could not be
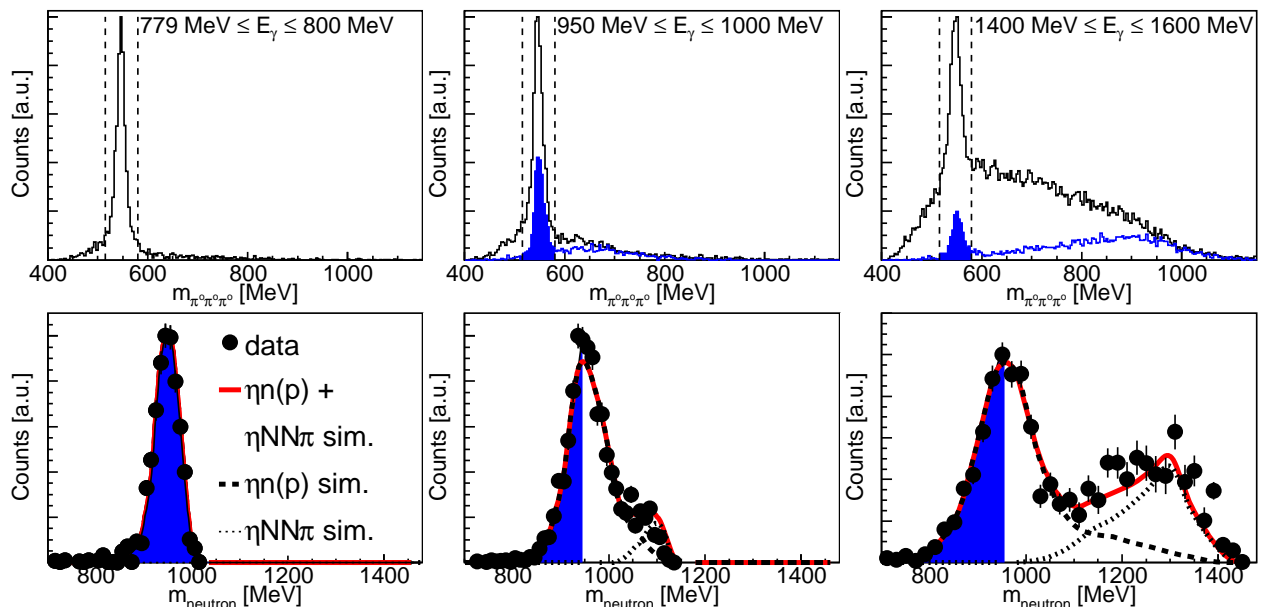

Figure 4: Upper part: 6-photon invariant mass spectra. Blue: after cut on missing mass. Lower part: missing mass spectra. Dashed lines: simulation of peak line shape (tail from large Fermi momenta), dotted: simulation of background from $\eta\pi$ final states. Red solid: sum of both.

used due to the fact that only the TAPS detector could trigger on photons, so that only events with

photons in this limited solid angle could be investigated. The $\gamma d \to p(n)\eta$ and $\gamma d \to (p)n\eta$ (in brackets: spectator nucleon) have been identified via invariant mass and missing mass analysis for the η-meson and identification of charged particles with the Barrel-Inner detector and the TAPS veto-detectors. Neutrons in TAPS could be identified with time-of-flight versus energy. Neutrons in the barrel where identified in events with 7 neutral hits by first assigning 6 hits via a χ^2 analysis to the decays of the three π^o mesons and then taking the left-over hit as tentative neutron. Typical invariant mass spectra are shown in the upper row of fig. 4 for three typical regions of incident photon energies for reactions with coincident recoil neutrons. At low incident photon energies, they show basically background free invariant mass peaks of the η meson. At higher incident photon energies background mainly due o the $\eta\pi^o$ final state appears in the spectra. This background was removed by using the the kinematical over-determination of the reaction for a missing mass analysis (the momentum distribution of the nucleons bound in the deuteron can be neglected, since it only results in a moderate broadening of the missing mass structures. Typical missing mass spectra after a cut on the η invariant mass are shown in the lower part of fig. 4. A very stringent cut accepting only events in the left half of the missing mass peak was applied to avoid any contamination from $\eta\pi$ final states that could produce artificial structure in the excitation functions. The small background remaining in the invariant mass spectra after the missing mass cut was determined by fits using the simulated invariant mass line-shapes and a background polynomial.

This data was divided into three sub-samples: η-meson in coincidence with recoil protons (σ_p), η-mesons in coincidence with recoil neutrons (σ_n), and η mesons without any condition on recoil nucleons (σ_{np}), including the first two sub-samples but also all events were the recoil nucleon was not detected. Since coherent production of η mesons off the deuteron in this energy range is completely negligible, this allowed to construct the quasi-free neutron cross section in two independent ways: directly via identification of the recoil neutron (σ_n), or indirectly as $\sigma_{np} - \sigma_p$. Since σ_n depends on the simulated detection efficiency for neutrons while $\sigma_{np} - \sigma_p$ depends on the proton detection efficiency this provides a very stringent test of possible systematic uncertainties for the nucleon detection efficiencies.
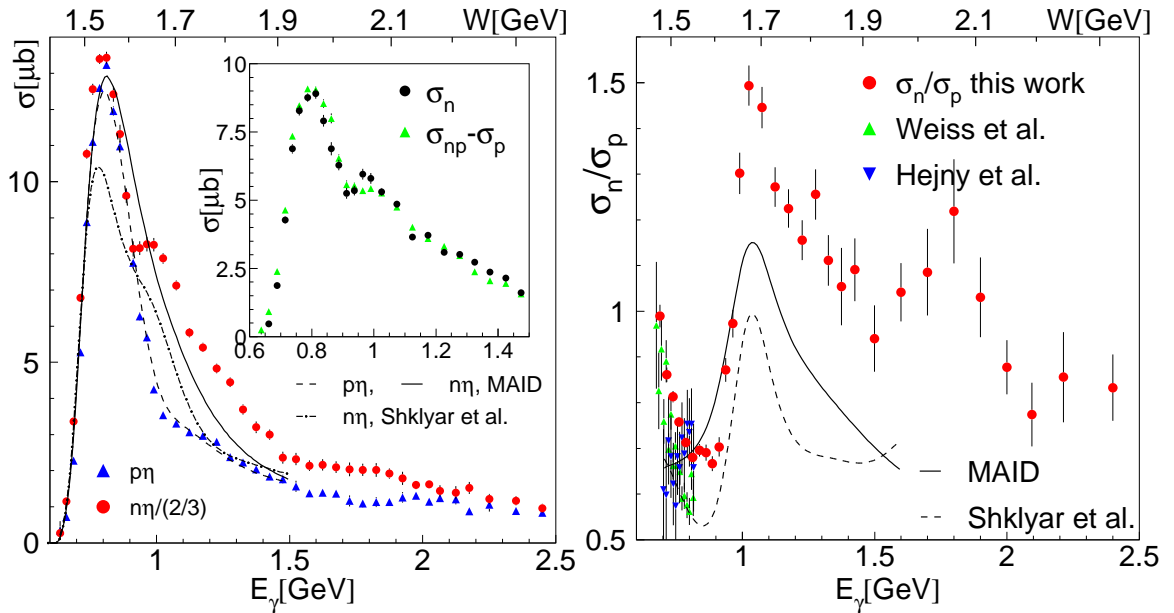

Figure 5: Left hand side: quasi-free cross sections off proton and neutron. Curves: model predictions MAID model [19], and Shklyar et al. [31]), all folded with Fermi motion. Neutron data and curves are scaled up by a factor of $3/2$. Insert: comparison of neutron cross sections from different analyses (see text). Right hand side: neutron/proton cross section ratio. Old low energy data from Refs. [14, 11]

Total cross sections of the quasi-free reactions off protons and neutrons are summarized in fig. 5. In the neutron excitation function indeed a narrow structure is seen at incident photon energies around 1 GeV, resulting in a sharp peak in the cross section ratio, which is of course broadened by Fermi smearing. A second, broader structure may be visible around 1.8 GeV. The insert in the figure at the

left hand side demonstrates the excellent control of systematic uncertainties for the neutron excitation function. It should be stressed that an explanation of the structure in the neutron excitation function via any kind of FSI or re-scattering effects is extremely unlikely since the proton excitation function at the same incident photon energy (see fig. 1) does not show any indication of such effects. Therefore it is almost certainly a genuine structure in the excitation function of the free neutron, broadened here by Fermi smearing.
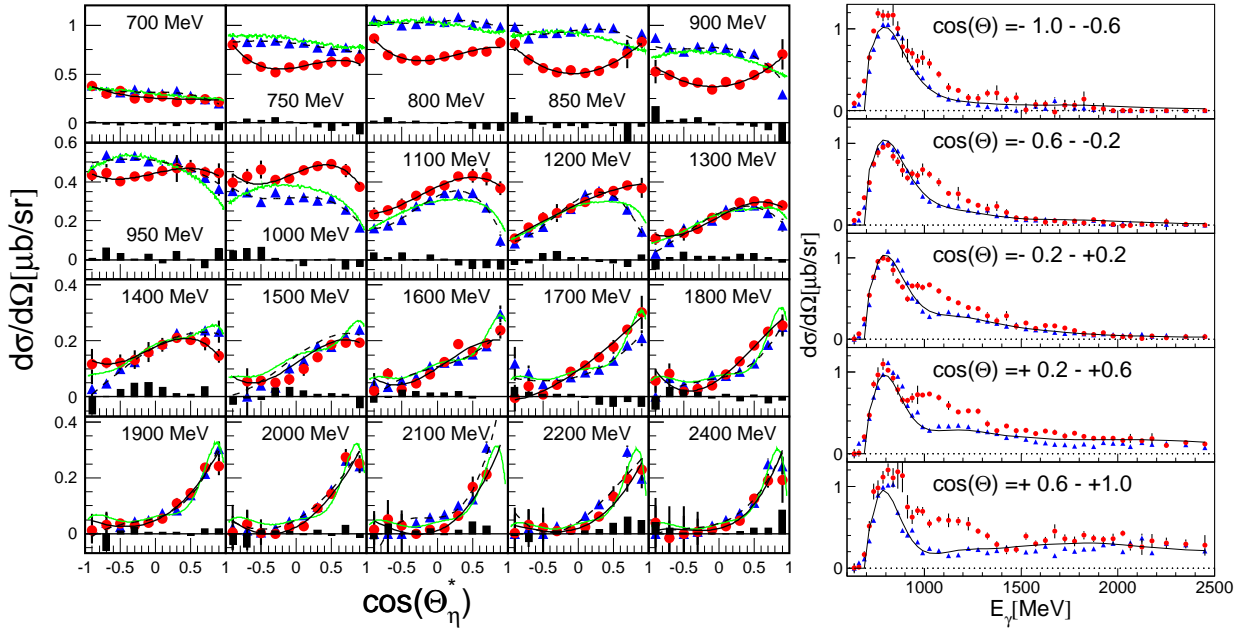
Figure 6: Left hand side: angular distributions for the reaction of the quasi-free neutron (red circles) and the quasi-free proton (blue triangles). Black curves: fits to the distributions, green curves: Fermi smeared cross section off the free proton. Bar charts: differences between σ_n and $\sigma_{np} - \sigma_p$ (neutron results are averages of these). Right hand side: excitation functions for different angular bins.

Angular distributions are summarized in fig.6. They have been fitted with with Legendre polynomials $P_i(cos(\Theta_\eta^\star))$, related to the contributing partial waves [4]:

$$\frac{d\sigma}{d\Omega} = \frac{q_\eta^\star}{k_\gamma^\star} \sum_i A_i P_i(cos(\Theta_\eta^\star)) \tag{5}$$

where the A_i are expansion coefficients. The results for $A_0, ..., A_4$ are shown in Fig. 7. In the region of the dominant $S_{11}(1535)$, the s-wave contributions (A_0) reflect the ratio of the helicity couplings of this resonance [4], and the shape of the angular distributions reflects the interference with the $D_{13}(1520)$ (see Ref. [14]). In this region, the angular distributions for proton and neutron are well described by the MAID model [19], which qualitatively reproduces the peak in the A_2 coefficient due to the S_{11} - D_{13} interference. The angular distributions for protons and neutrons are similar for high incident photon energies, where diffractive t-channel processes make a large contribution [23, 34]. In the most interesting region around $E_\gamma \approx 1$ GeV, the shapes of the angular distributions for the neutron and the proton change rapidly, and apart from A_0, their Legendre coefficients become similar. For the proton, the A_1 coefficient rises sharply from negative to positive values. Denizli et al. [33] have recently shown in electro-production that this feature survives to larger Q^2 values, and interpreted it as an interference between S_{11} and P-resonances. This is also in agreement with our previous data for the free proton [23, 34], where a strong contribution from $P_{13}(1720)$ was found in this region. However, it should be stressed that an interference between S- and P-resonances cannot produce the bump-structure in the total cross section since the interference term $\propto cos(\Theta)$ in the angular distributions integrates out in the total cross section. It is nicely visible in the left hand side of fig. 6 that the bump structure is seen for all angular bins.

Due to the effects of the Fermi smearing so far, no definitive conclusion could be drawn to the nature of this structure. Fix, Tiator, and Polyakov [35] find comparable results for the MAID model with
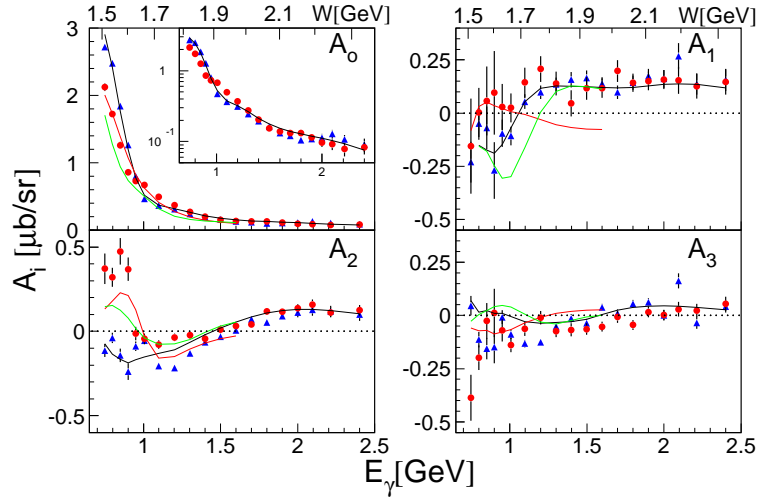
Figure 7: Legendre coefficients of angular distributions. Red circles: quasi-free neutron, blue triangles: quasi-free proton, Curves: free proton data [23] (black), Maid neutron [19] (red), Shklyar et al. neutron [31] (green), all folded with Fermi motion. Insert: logarithmic scale for A_0.

strong D_{15} contribution and for a model with a P_{11} resonance as narrow as 10 - 30 MeV. Anisovich et al. [36] have also discussed different scenarios, which are summarized in fig. 8 Reasonable fits to
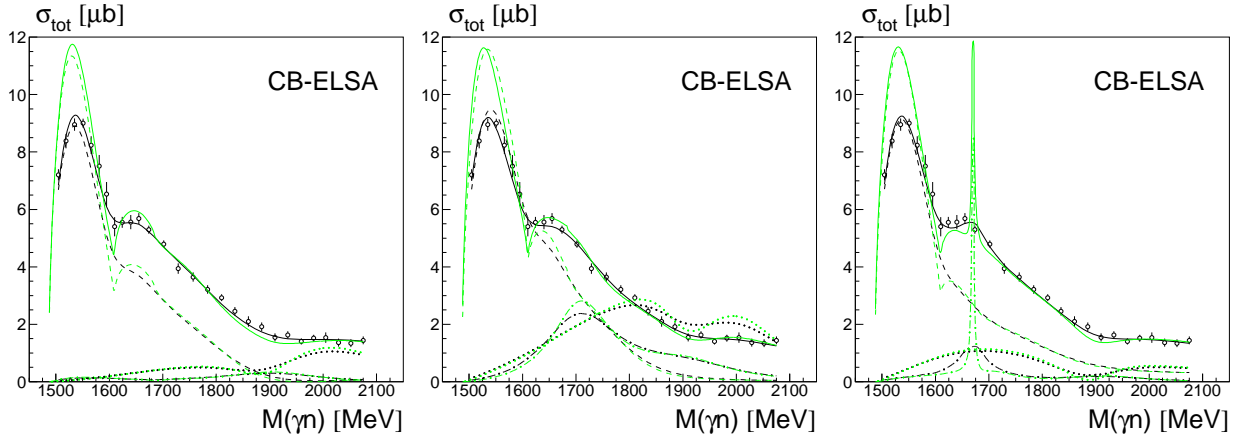

Figure 8: In all sub-figures green curves refer to free neutron cross sections, black curves to Fermi smeared cross sections. Left hand side: solution from fine-tuning of interference between S_{11} resonances. Center: introduction of a wide P_{11} resonance, right hand side: introduction of a narrow P_{11} resonance.

the total cross section and angular distributions are obtained for fits with special fine-tuning of the interference structure between resonances and resonances and background in the S_{11} sector, for the enforcement of a broad P_{11} resonance or a very narrow P_{11} resonance, which due to Fermi smearing produce similar effects.

The next important step on the experimental side was therefore a better estimate of the intrinsic width of the structure for the free neutron. A crude estimate was obtained from the ELSA-data in the following way. The excitation functions predicted from the MAID model [19] were folded with the nucleon momentum distributions calculated from the deuteron wave function. In both cases we have calculated approximate correction factors from the ratio of folded and unfolded distributions and applied them to the data. Since the MAID results for the proton are in excellent agreement with the data, the correction is precise for the proton, but strongly model dependent for the neutron. The result is shown at the right hand side of 9. Below energies of 900 MeV, proton and neutron data have identical shapes. A fit in this energy range with a Breit-Wigner parameterization like in [32] reproduces the $S_{11}(1535)$ parameters extracted from photoproduction off the free proton. It yields W=1538 MeV

for proton and neutron data, Γ=157 (proton), Γ=148 MeV (neutron), and $A^p_{1/2}$=103, $A^n_{1/2}$=85 in units of $10^{-3}\mathrm{GeV}^{-1/2}$. In the cross section ratio, the peak around 1 GeV is more pronounced and narrow than in the uncorrected data, but this is still only an upper limit for the true width of this structure. In principle, Fermi motion can be corrected event-by-event when energy and momentum of
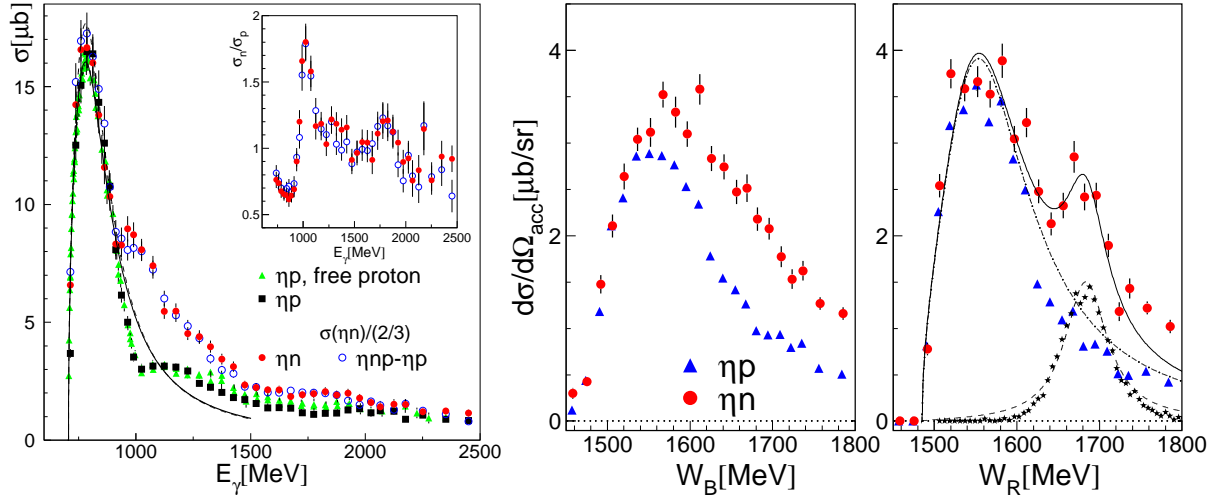

Figure 9: Left hand side: approximate correction of total cross sections from Fermi smearing. Right hand side: Proton and neutron excitation functions for $cos(\Theta^\star_\eta) < -0.1$ without (invariant mass W_B from incident photon energy) and with (invariant mass W_R from neutron - η 4-vectors) event-by-event correction of Fermi motion. Curves: solid: full fit, dash-dotted: BW-curve of $S_{11}(1535)$, dashed: BW-curve for second structure. Stars: response for a δ-function due to finite energy resolution.

the recoil nucleons are known. Instead of using the total cm energy W_B deduced from the incident photon energy, it can be reconstructed as final state invariant mass from the four-vectors of the η meson and the recoil nucleon (W_R). Since the energy of the neutrons was measured by time-of-flight, only neutrons in TAPS, which correspond to η mesons with $\cos(\Theta^\star_\eta) < -0.1$ were used. The results are shown in fig. 9. For proton and neutron, the correction leads to the expected narrower peak for the $S_{11}(1535)$. However, for the neutron also a narrow structure around $W \approx 1.7$ GeV appears. The neutron data was fitted with the sum of two Breit-Wigner (BW) curves corresponding to the $S_{11}(1535)$ and the structure around 1.7 GeV. The parameters for the S_{11} (position: 1566 MeV, width: 162 MeV) are similar to a fit of the free proton data (1540 MeV, 162 MeV). The position of the second structure (W=1683 MeV) is in agreement with the result of the GRAAL experiment ($W \approx 1.68$ GeV, [29]). The fitted width of this structure is (60±20) MeV, however, this is only an upper limit, since it is broadened by the time-of-flight resolution. Even the simulation of a δ-function at the peak position reproduces the observed line-shape (see Fig. 9), so that no lower limit of the width could be deduced. Consequently, the result is not in contradiction with the GRAAL experiment. However, the statistical quality of this data was very limited.

1.3 Very preliminary results from the MAMI A2-10 proposal

For the previous PAC meeting we had proposed (MAMI A2-10) to measure with much better statistics angular distributions and total cross sections and the double polarization observable E. The first part (angular distributions and excitation functions) has been measured in three different beam times, the last in May 2009. The data are currently under analysis. The measurement of E has to await availability of the polarized deuteron target.

Very preliminary results for the neutron excitation function are shown in fig. 10. Again they are obtained once as function of W calculated from the incident photon energy (i.e. broadened by Fermi motion) and once as function of W calculated from the η, neutron four vectors (i.e. not broadened by Fermi motion but by experimental resolution). The statistical quality of the data (only part of the available data is included in the figure) is much better than in the previous ELSA experiment. This
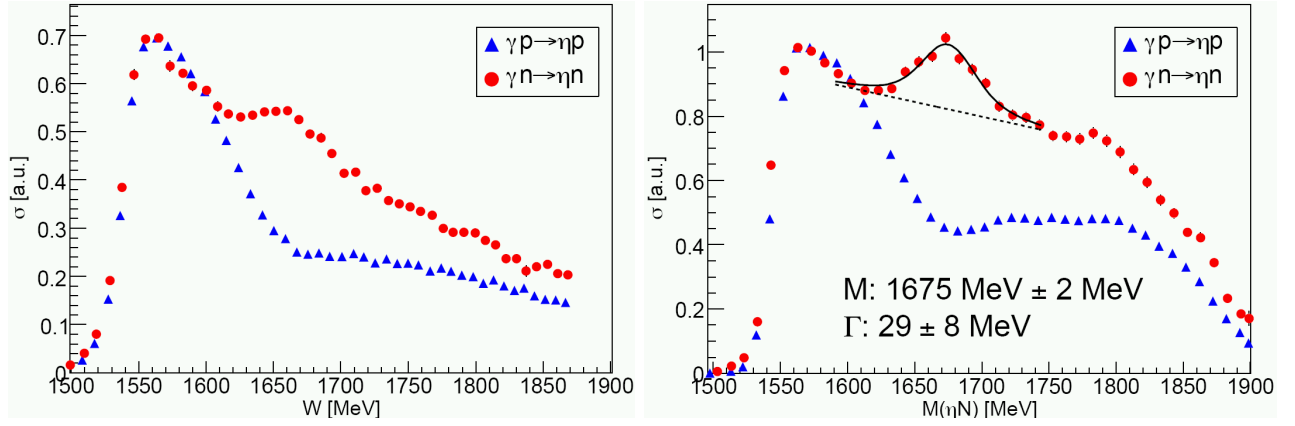
Figure 10: Very preliminary results for the excitation function of the neutron without correction for experimental efficiency and analysis cuts. Left hand side: excitation functions as function of W calculated from incident photon energy. Right hand side: W calculated as ηn final state invariant mass. Line: fit with Breit-Wigner folded with experimental resolution.

is mainly due to the fact that in contrast to the Crystal Barrel the Crystal can trigger on photons, which has the additional advantage, that the two-photon decay channel of the η meson can be used, giving better resolution for the η four-vectors. Again, the structure becomes more pronounced, when Fermi motion is eliminated. In this case the neutron four-vectors are not based on a time-of-flight measurement, but are derived from the over-determined reaction kinematics, using only the angle measurement of the neutron. However, for neutrons detected in TAPS, time-of-flight information could further improve the resolution in a kinematic fitting procedure, which will be done in a later state of the data analysis. The data have been fitted with a Breit-Wigner curve folded with the experimental resolution. The fit results in a Breit-Wigner width of (30 ± 8) MeV, confirming that in case the structure would be related to a nucleon resonance, it must have very unusual properties.

1.4   Summary of properties of structure in neutron excitation function

- **The structure has been observed in photoproduction of η-mesons off neutrons bound in the deuteron at:**

  - **GRAAL in Grenoble [28, 29] with $\Gamma < 30$ MeV**
  - **ELSA in Bonn [9] with $\Gamma < 60$ MeV**
  - **Tohoku-LNS [37] with $\Gamma < 40$ MeV**
  - **MAMI Mainz [38] with $\Gamma < 40$ MeV**

- **it is extremely unlikely that the structure is caused by 'deuteron' effects like FSI, re-scattering, since in the same energy region there is no observable effect for the proton case where free and quasi-free reaction can be compared.**

- **it can not be solely due to an S - P interference since a pronounced bump appears in the total cross section**

- **so far no information about the responsible partial wave has been obtained.**

- **although the $D_{15}(1675)$ resonance is not a likely cause of the narrow structure, it is not ruled out that a significant contribution from this state in addition to the narrow structure causes the much slower fall-off of the neutron cross section in this energy region compared to the proton.**

1.5 Sensitivity of polarization observables

With the availability of circularly and linearly polarized photon beams combined with longitudinally and transversely polarized targets access to all single polarization observables (the recoil polarization observable P can be measured in the combination linearly pol. beam, transversely pol. target) and all double polarization observables of the beam - target type is given. The general form of the differential cross section is given in this case as [39]:

$$
\begin{aligned}
\frac{d\sigma}{d\Omega} \;=\; \frac{d\sigma}{d\Omega}\Big|_{unpol.} \quad & \cdot\{1 - P_{lin}\Sigma\cos(2\Phi) \\
& + P_x[-P_{lin}H\sin(2\Phi) + P_{circ}F] \\
& - P_y[+P_{lin}P\cos(2\Phi) - T] \\
& - P_z[-P_{lin}G\sin(2\Phi) + P_{circ}E]\}
\end{aligned}
\tag{6}
$$

P_{lin}, P_{circ} are the linear and longitudinal polarization degrees of the photon beam, (P_x,P_y,P_z) is the polarization of the target and Φ is the angle between the reaction plane and the linear polarization of the beam. Consequently, with four measurements combining circularly polarized beam and longitudinally polarized target (E), circularly polarized beam and transversely polarized target (F,T), linearly polarized beam and longitudinally polarized target (Σ, G), and linearly polarized beam and transversely polarized target (P,H) seven polarization observables can be measured.

It must be emphasized that for model analyses in terms of the photoproduction mutlipoles it is extremely important to have experimental input for a reasonably large set of different polarization observables. In this sense, it is often more efficient to measure a couple of different polarization observables with moderate statistical uncertainties rather than to measure one or two observables with very high accuracy.
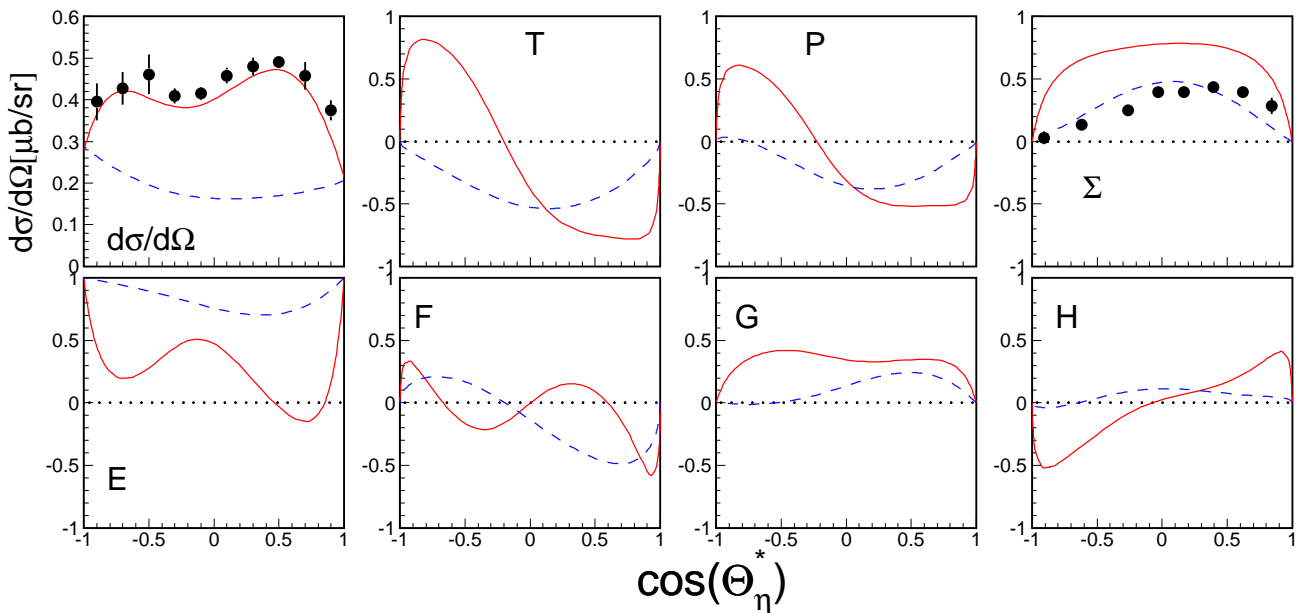

Figure 11: Predicted asymmetries from the η-MAID model at E_γ=1 GeV. Solid, red curves: full model, dashed, blue curves without D$_{15}$(1675) resonance. Black dots: experimental results for differential cross section (ELSA) [9] and Σ (GRAAL) [40]

In the following, we will shortly discuss the expected magnitude of the polarization observables and their sensitivity to different resonance contributions. Since so far the resonance contributions to $\gamma n \to n\eta$ in the energy range in question is simply unknown, we can give only some reasonable expectations from the predictions of the η-MAID model [19]. In fig. 11 the predictions from the full model are compared to a model version that excludes the D$_{15}$(1675) resonance. The model has not been refitted after exclusion of the D$_{15}$, so that this results must be taken with some care, however they are sufficient for the demonstration of the qualitative behavior of such a truncated model version. The

model predicts asymmetries of measurable size for basically all polarization observables. The effect of the D_{15} resonance, which in this model at the energy range in question is the only state with spin larger than $1/2$ that significantly contributes, is clearly visible for all observables. However, so far the situation even in view of this state is completely unclear. While the ELSA-data for the differential cross section clearly favor the model version with large D_{15} contribution, the GRAAL-data for the linear beam asymmetry Σ are in better agreement with the truncated model.

Figs. 12,13 summarize the expected experimental sensitivity for the experiments suggested for MAMI and ELSA, angular dependencies
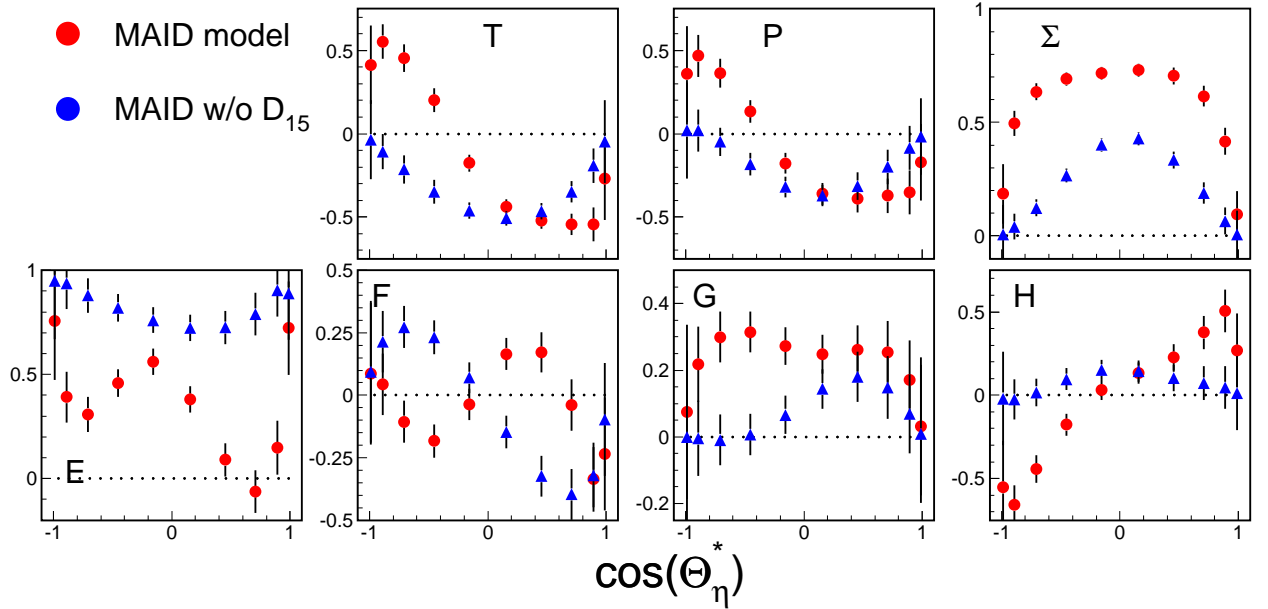
Figure 12: Expected sensitivity of the proposed measurements at ELSA (P,Σ,G,H) and MAMI (T,E,F) at incident photon energy of 1020 MeV. Red circles full MAID model, blue triangles: MAID without D_{15}.
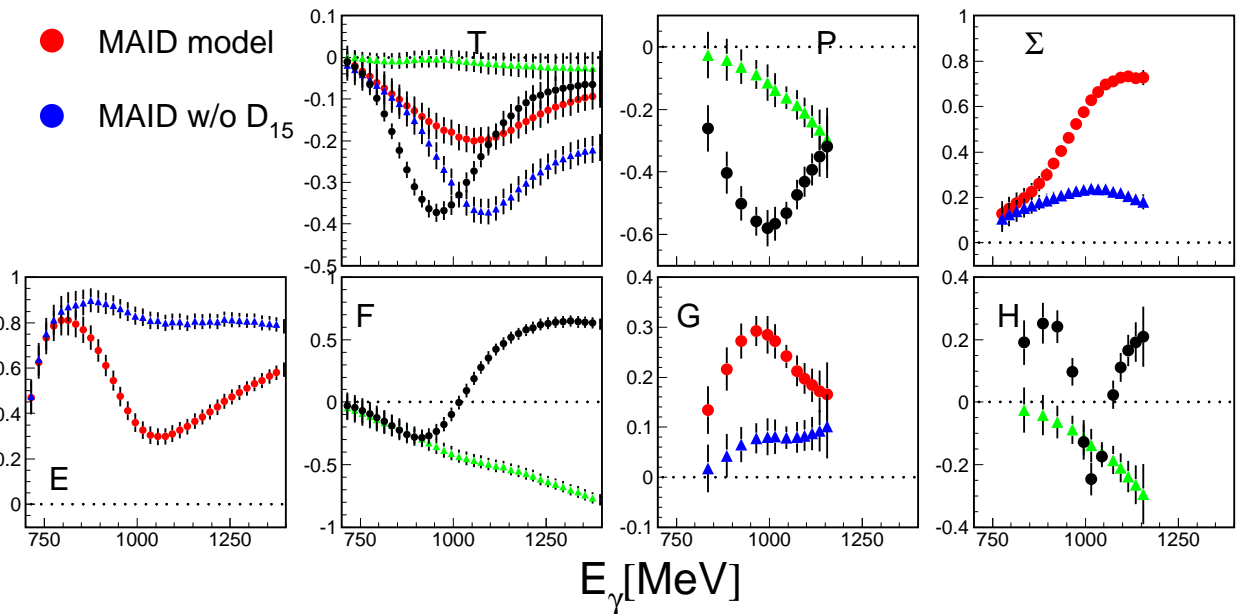
Figure 13: Expected sensitivity of the energy dependence of the angle integrated asymmetries. Red circles full MAID model, blue triangles: MAID without D_{15}. Black and green symbols: same but asymmetries for $\cos(\Theta) < 0$ multiplied by -1 before integration.

at E_γ=1020 MeV in fig. 12 and integrated energy dependencies in fig. 13. For some observables, due to the particular angular dependence the sensitivity of the energy integrated observables is much larger when the values at $\cos(\Theta) < 0$ are multiplied by -1 before integration (P,F,H). For T normal integration gives larger asymmetries for the full MAID model, the other version for the truncated model.
These results have been obtained using:

- **measured differential cross sections (ELSA-experiment) [9]**

- **predictions for the polarization observables from the η-MAID model**

- **full Monte Carlo simulations of the experimental detection efficiencies**

- **smearing of the observables by nuclear Fermi motion**

- **the further experimental details like polarization degrees etc. discussed separately for the ELSA and MAMI experiments in the experiment section**

- **the following total beam times:**
    - **MAMI: circularly pol photons, longitudinally pol. target:**   **700 h**
    - **MAMI: circularly pol photons, transversely pol. target:**   **700 h**
    - **ELSA: linearly pol photons, longitudinally pol. target:**   **1400 h**
    - **ELSA: linearly pol photons, transversely pol. target:**   **1400 h**

The estimates shown above give only an overall summary of the expected results, detailed results for the different observables are given in the appendices of the two proposals.
It should be emphasized that prompted by the puzzling situation for the $\gamma n \to n\eta$ reaction, here we have only concentrated on the topic of η-production. It is however evident, that simultaneously results of similar quality will be obtained for other reaction channels with at least comparable cross sections (total coss section for the η channel in the region of interest ≈ 5 μb), i.e.for example for π^o production or double pion production channels. Partly, measurements for this channels overlap with other proposals.

2 Proposed experiments

2.1 General considerations

We propose to measure for quasi-free photoproduction off neutrons bound in the deuteron the polarization observables E,T,F with circularly polarized photons at MAMI C in Mainz and the polarization observables Σ, G, P, H with linearly polarized photons at ELSA in Bonn. Both experiments require measurements with a longitudinally polarized target and a transversely polarized target.

The proposed experiments require the following beam/target combinations:

- **E: circularly polarized beam, longitudinally polarized target (MAMI C)**

- **T,F : circularly polarized beam, transversely polarized target (MAMI C)**

- **Σ, G: linearly polarized beam, longitudinally polarized target (ELSA)**

- **P, H: circularly polarized beam, transversely polarized target (ELSA)**

The observable Σ could of course also measured with unpolarized target and T with unpolarized beam, however it is more efficient to due them in parallel with the other observables. This means no loss in quality for T, where simply the information of the circular beam polarization can be ignored. In case of Σ some degration due to the target dilution is compensated by the long beam time for the measurement with the polarized target.

The measurements with linearly polarized beam have to be done at ELSA since at MAMI the polarization degree at incident photon beam energies around 1 GeV is too low due to the lower electron beam energy (see Appendix A). The experiments with circularly polarized beams are planned for MAMI for two reasons. First, the usable photon flux is higher at MAMI and secondly the Crystal Barrel detector in Bonn must be upgraded for trigger capability before measurements off the neutron can be done efficiently (see Proposal Part II).

In this section we discuss only some further experimental issues common for both experiments. Details of the individual experiments are given separately in the next section for both proposal.
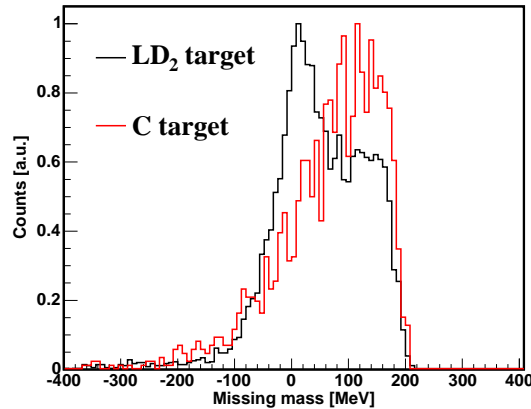
Figure 14: Missing mass spectra for the reaction $\gamma n \to n\eta$ for a deuteron and a carbon target at 1 GeV incident photon energy (arbitrary units)

Both experiments will use polarized frozen spin targets consisting of solid deuterated butanol ($C_4D_{10}O$). The polarization is diluted by the unpolarized neutrons from the carbon and oxygen nuclei. By simply counting the number of polarized and unpolarized neutrons a dilution factor of

$$f_o = \frac{10}{42} = 0.24 \tag{7}$$

is obtained. This is however to pessimistic, first the cross sections off nuclei do not scale with the mass number (due to FSI effects), secondly a significant part of the unpolarized background can be removed with cuts on the reaction kinematics ('missing mass') since due to Fermi motion and final state interaction this spectra are more broadened for the photoproduction off C, O compared to the deuteron. Typical missing mass spectra for η production from the deuteron and from carbon at an incident photon energy of 1 GeV measured with the Crystal Barrel and TAPS at ELSA in coincidence with recoil neutrons are shown in fig. 14. The effective dilution factor can be determined by a comparison of these spectra. It is estimated by:

$$f_{eff} = \frac{10 \cdot N_d}{10 \cdot N_d + 16/3 \cdot N_C} \tag{8}$$

where N_d, N_C are the counts normalized to the photon flux and number of target nuclei in the window around zero that will be used for the analysis. Due to the chemical composition of butanol deuterium enters with a weight of 10. Carbon enters with a weight of 4, and oxygen is scaled as 8/6 of carbon, so that the unpolarized neutrons contribute with 16/3 of the carbon cross section. The effective dilution factors calculated this way range between 0.8 and 0.5 for incident photon energies from 0.7 to 1.5 GeV on average we assume f_{eff}=0.7. We assume the same reduction factor for the background from the target windows, which without cuts contributed C=4 in the GDH experiments. This corresponds to relative background contributions to the count rates of $B = 1/f - 1$=0.43 for the butanol and C=0.54 for the target cell. With this the total dilution of the asymmetry is estimated as:

$$\eta = 1 + B + C \approx 2 \quad . \tag{9}$$

2.2 Measurements with Crystal Ball/TAPS at MAMI C

The MAMI C part of the experiment (E,T,F) requires two separate measurements both using circularly polarized photon beam combined with th longitudinally and transversely polarized targets, which will be available at MAMI C during 2010. The experimental setup consisting of the Crystal Ball (with PID) and the TAPS forward detector will be identical in both experiments and corresponds to the standard setup described in Appendix A of this proposal, where all relevant details are given. For all measurements the $\eta \to \gamma\gamma$ decay channel will be used (some additional statistics may be obtained from the $\eta \to 3\pi^o \to 6\gamma$ decay channel, however, with somewhat lower experimental resolution for the kinematical variables of the η). The sensitivity and accuracy of the proposed measurements has been studied in detail (see Appendix B) with Monte Carlo simulations of the achievable detection efficiency of the apparatus including detection of the recoil nucleons. The simulations have been tested with the already available quasi-fee neutron data from unpolarized targets. For the proposed experiments we aim at a maximum statistical uncertainty for the double polarization observables of 0.15 for a minimum cross section of 0.35 in 40 MeV bins of incident photon energy. The necessary beam time can be derived from the statistical accuracy using:

$$\delta A_{stat}^2 = (1 - A^2) \cdot \eta [\Delta t \cdot P^2 \cdot N_\gamma \cdot N_T \cdot l_f \cdot \epsilon \cdot b \cdot \Delta\sigma_o]^{-1} \tag{10}$$

with the following notation (energy dependent quantities are given for an incident photon energy of 1 GeV):

- A: measured asymmetry

- δA_{stat}: statistical uncertainty of $A \Rightarrow$ **0.15**

- N_γ: number of photons per 40 MeV incident photon energy (including tagging efficiency) $\Rightarrow$ **4.6· 10^5sec^{-1}**

- N_T: surface density of target nuclei (2 cm frozen butanol target) $\Rightarrow$ **0.09 b^{-1}**

- l_f: data taking life time $\Rightarrow$ **0.7**

- ϵ: detection efficiency, assumed on average as $\Rightarrow$ **0.07**

- b: decay branching ratio of η mesons, for $\eta \to 2\gamma \Rightarrow$ **0.4**

- $\Delta\sigma_o$: unpolarized cross section in the respective angular bins.
  We assume minimal $\Rightarrow \Delta\sigma_o$=**0.35 μb**

- P: product of polarization degrees $\Rightarrow P_t \cdot P_b=$ **0.7×0.5=0.35**

- $\eta = 1 + B + C$ effective dilution from unpolarized background $\Rightarrow$ **2.0**

The resulting beam time request is:

- **700 h** circularly polarized beam, longitudinally polarized target
- **700 h** circularly polarized beam, transversely polarized target

The expected results for this beam time are summarized in Appendix B.

3 Appendix A: Experimental apparatus

3.1 Photon Beam

The A2 photon beam is derived from the production of Bremsstrahlung photons during the passage of the MAMI electron beam through a thin radiator. The resulting photons can be circularly polarised, with the application of a polarised electron beam, or linearly polarised, in the case of a crystalline radiator. The degree of polarisation achieved is dependent on the energy of the incident photon beam (E_0) and the energy range of interest, but currently peaks at $\sim$75% for linear polarisation (Fig. 15) and $\sim$85% for circular polarisation (Fig. 16). The maximum degree of linear polarisation should be further improved by 5 to 10% by the end of 2009 when the collimation and beam monitoring systems will be optimised for MAMI-C during the installation of the Frozen Spin Target. The Glasgow Photon Tagger (Fig 17) provides energy tagging of the photons by detecting the post-radiating electrons and can determine the photon energy with a resolution of 2 to 4 MeV depending on the incident beam energy, with a single-counter time resolution $\sigma_t = 0.117$ ns [42]. Each counter can operate reliably to a rate of $\sim$1 MHz, giving a photon flux of $2.5 \cdot 10^5$ photons per MeV. Photons can be tagged in the momentum range from 4.7 to 93.0% of E_0.
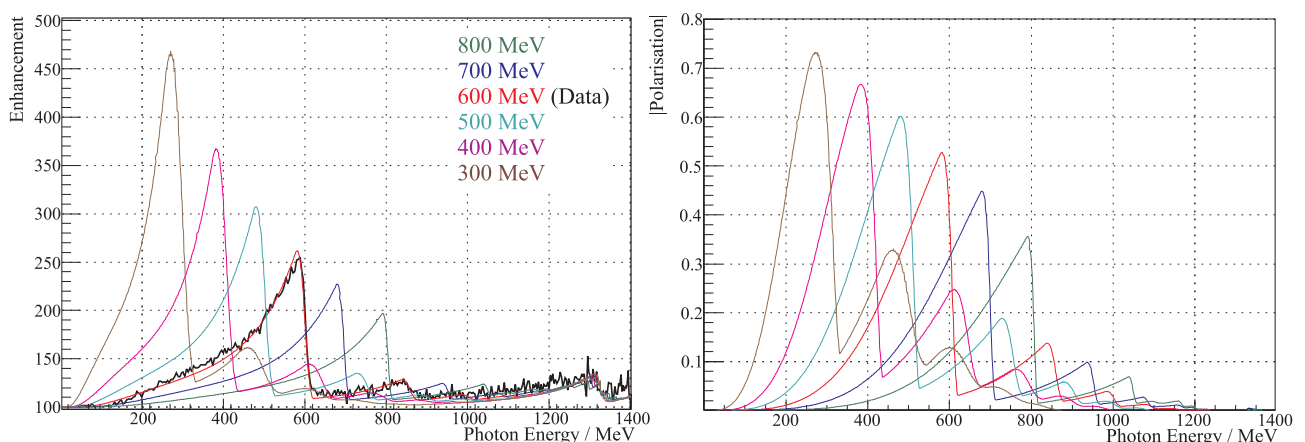

Figure 15: Linear polarisation available with the current collimation system for a variety of crystal orientations. The thin black lines are data obtained during recent MAMI-C runs.
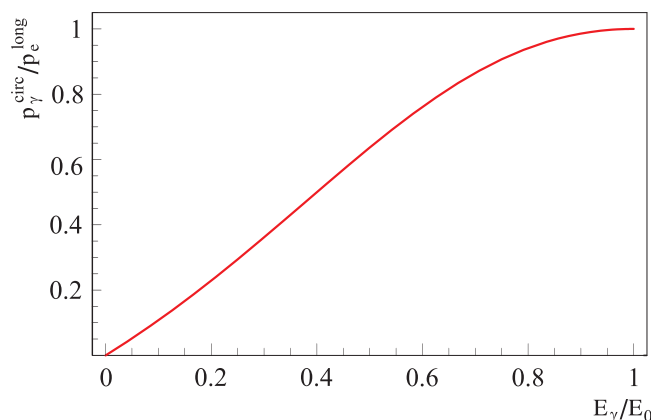

Figure 16: Helicity transfer from the electron to the photon beam as function of the energy transfer. The MAMI beam polarisation is $P_e \approx$85%.

To augment the standard focal plane detector system and make use of the Tagger's intrinsic energy resolution of 0.4 MeV (FWHM), there exists a scintillating fibre detector ('Tagger Microscope') that can improve the energy resolution by a factor of about 6 for a $\sim$100 MeV wide region of the focal plane (dependent on its position) [44].
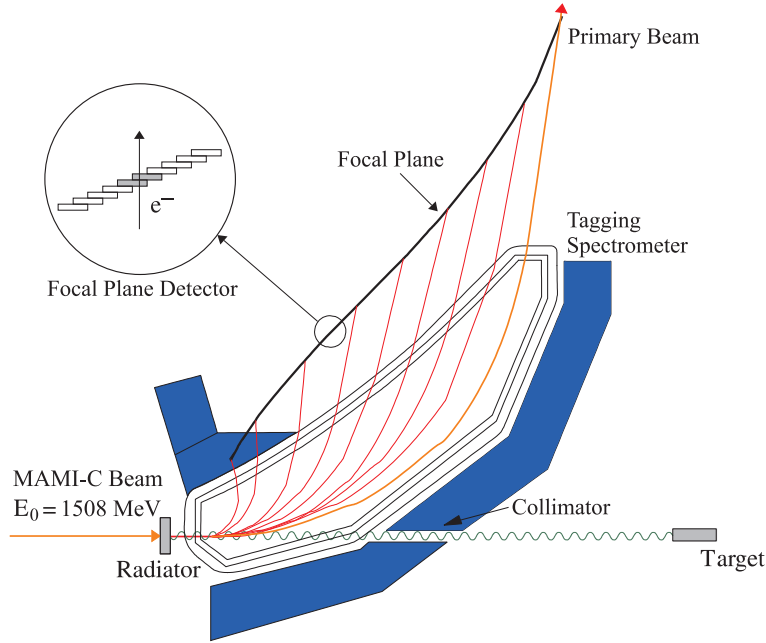
Figure 17: The Glasgow photon tagging spectrometer.

3.2 Frozen-Spin Target

Polarisation experiments using high density solid-state targets in combination with tagged photon beams can reach the highest luminosities. For the double polarisation measurements planned with the Crystal Ball detector on polarised protons and deuterons a specially designed, large horizontal ^{3}He/^{4}He dilution refrigerator was built in cooperation with the Joint Institute for Nuclear Research (JINR) Dubna (see Figure 18). It has minimum limitations for the particle detection and fits into the central core of the inner Particle Identification Detector (PID2). This was achieved by using the frozen spin technique with the new concept of placing a thin superconducting holding coil inside the polarisation refrigerator. Longitudinal and transverse polarisations will be possible.

Highest nucleon polarisation in solid-state target materials is obtained by a microwave pumping process, known as 'Dynamic Nucleon Polarisation' (DNP). This process is applicable to any nucleus with spin and has already been used in different experiments with polarised proton and deuteron targets. The geometric configuration of the target is the same for the polarised proton and neutron setup. However, since the polarisation measurement of the deuteron is more delicate due to the small size of the polarisation signals, the modification of some basic components is needed. The reason for this is twofold: firstly the magnetic moment of the deuteron is smaller than that of the proton and, in addition, the interaction of the deuteron quadrupole moment with the electric field gradient in the sample broadens the deuteron polarisation signal. An accuracy $\delta P_p/P_p$ of 2 to 3% for the protons and $\delta P_D/P_D$ of 4 to 5% for the deuterons is expected in the polarisation measurement. It has also to be taken into account that the measured deuteron polarisation P_D is not equal to the neutron polarisation P_n. Assuming a 6 % admixture of the D-state of the deuteron, a calculation based on the Clebsch-Gordon coefficients leads to $P_n = 0.91 \, P_D$. Several polarised proton and deuteron materials are available such as alcohols and deuterated alcohols (e.g. butanol C_4H_9OH), NH_3, ND_3 or ^{6}LiD. The most important criteria in the choice of material suitable for particle physics experiments are the degree of polarisation P and the ratio k of free polarisable nucleons to the total number of nucleons. Further requirements on polarised target materials are a short polarisation build-up time and a simple, reproducible target preparation. The polarisation resistance against radiation damage is not an issue for experiments with a low intensity tagged photon beam ($\dot{N_\gamma} \approx 5 \cdot 10^7$ s^{-1}) as will be used here. However, the limitations of a reduced relaxation time due to overheating of the target beads (Kapitza resistance) will have to be investigated.

Taking all properties together, butanol and deuterated butanol are the best material for this experiment. For protons we expect a maximum polarisation of $P_p = 90\%$ and an average polarisation of

Figure 18: The new dilution refrigerator for the Crystal Ball Frozen Spin Target.

$P_p = 70\%$ in the frozen spin mode. Recently, a deuteron polarisation $P_D = 80\%$ was obtained with Trityl doped butanol targets at 2.5 T magnetic field in a ^{3}He/^{4}He dilution refrigerator. At a 0.4 T holding field an average neutron polarisation P_n (see above) of 50 % will be obtained. The filling factor for the ~2 mm diameter butanol spheres into the 2 cm long, 2 cm diameter target container will be around 60%. The experience from the GDH runs in 1998 [45] shows that, with a total tagged photon flux of $5 \cdot 10^7$, relaxation times of about 200 hours can be expected. The polarisation has to be refreshed by microwave pumping every two days.

In conclusion, we estimate that we will achieve the following target parameters:

- Maximum total tagged photon flux in the energy range of 4.7 to 93% of E_0: $\dot{N}_\gamma \approx 5 \cdot 10^7 \, \text{s}^{-1}$, with relaxation time of 200 hours.

- Target proton density in 2 cm cell: $N_T \approx 9.1 \cdot 10^{22} \text{cm}^{-2}$ (including dilution and filling factors)

- Average proton polarisation $P_p = 70\%$

- Target deuteron density in 2cm cell: $N_T \approx 9.4 \cdot 10^{22} \text{cm}^{-2}$ (including dilution and filling factors)

- Average neutron polarisation $P_n = 50\%$

3.3 Crystal Ball Detector System

The central detector system consists of the Crystal Ball calorimeter combined with a barrel of scintillation counters for particle identification and two coaxial multiwire proportional counters for charged particle tracking. This central system provides position, energy and timing information for both charged and neutral particles in the region between $21°$ and $159°$ in the polar angle (θ) and over almost the full azimuthal (ϕ) range. At forward angles, less than $21°$, reaction products are detected in the TAPS forward wall. The full, almost hermetic, detector system is shown schematically in Fig. 19 and the measured two-photon invariant mass spectrum is shown in Fig. 20.
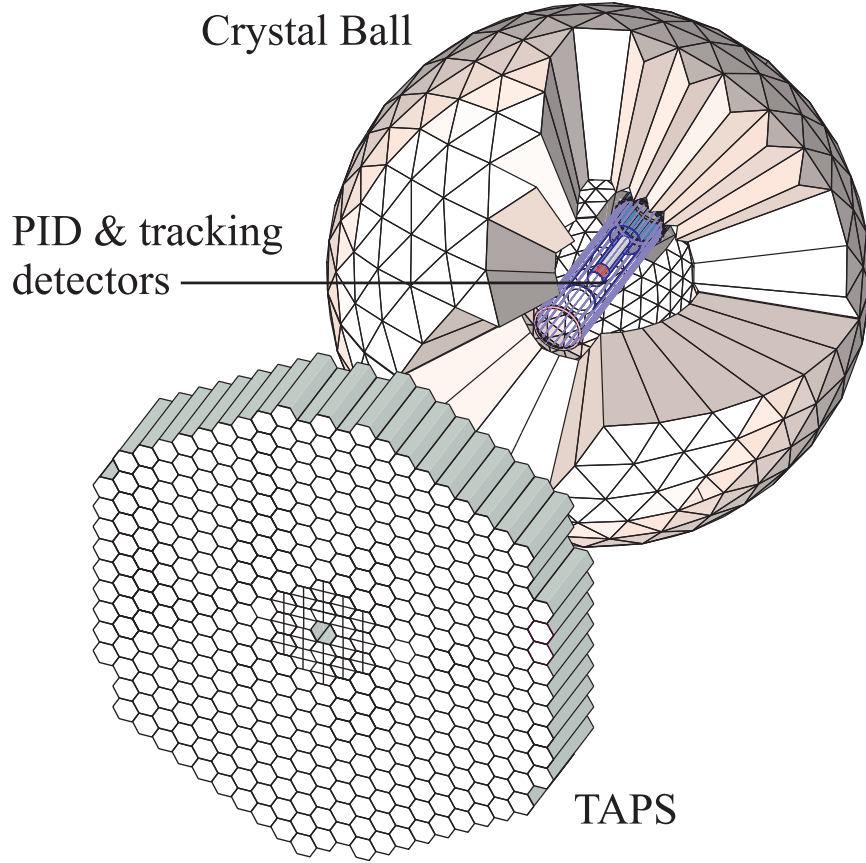
Figure 19: The A2 detector setup: The Crystal Ball calorimeter, with cut-away section showing the inner detectors, and the TAPS forward wall.

The Crystal Ball detector (CB) is a highly segmented 672-element NaI(Tl), self triggering photon spectrometer constructed at SLAC in the 1970's. Each element is a truncated triangular pyramid, 41 cm (15.7 radiation lengths) long. The Crystal Ball has an energy resolution of $\Delta E/E = 0.020 \cdot E[GeV]^{0.36}$, angular resolutions of $\sigma_\theta = 2 \ldots 3°$ and $\sigma_\phi = \sigma_\theta/\sin\theta$ for electromagnetic showers [41]. The readout electronics for the Crystal Ball were completely renewed in 2003, and it now is fully equipped with SADCs which allow for the full sampling of pulse-shape element by element. In normal operation, the onboard summing capacity of these ADCs is used to enable dynamic pedestal subtraction and the provision of pedestal, signal and tail values for each element event-by-event. Each CB element is also newly equipped with multi-hit CATCH TDCs. The readout of the CB is effected in such a way as to allow for flexible triggering algorithms. There is an analogue sum of all ADCs, allowing for a total energy trigger, and also an OR of groups of sixteen crystals to allow for a hit-multiplicity second-level trigger - ideal for use when searching for high multiplicity final states.

In order to distinguish between neutral and charged particles species detected by the Crystal Ball, the system is equipped with PID2, a barrel detector of twenty-four 50 mm long, 4 mm thick scintillators, arranged so that each PID2 scintillator subtends an angle of 15° in ϕ. By matching a hit in the PID2 with a corresponding hit in the CB, it is possible to use the locus of the $\Delta E, E$ combination to identify the particle species (Fig. 21). This is primarily used for the separation of charged pions, electrons and protons. The PID2 covers from 15° to 159° in θ.

The excellent CB position resolution for photons stems from the fact that a given photon triggers several crystals and the energy-weighted mean of their positions locates the photon position to better than the crystal pitch. For charged particles which deposit their energy over only one or two crystals, this is not so precise. Here the tracks of charged particles emitted within the angular and momentum acceptance of the CB detector will be reconstructed from the coordinates of point of intersections of the tracks with two coaxial cylindrical multiwire proportional chambers (MWPCs) with cathode strip readout. These MWPCs are similar to those installed inside the CB during the first round of MAMI-B
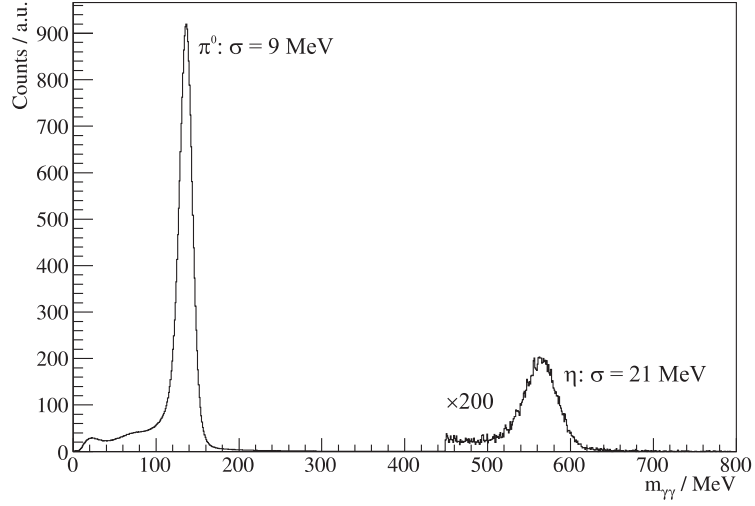
Figure 20: Two photon invariant mass spectrum for the CB/TAPS detector setup. Both η and π^0 mesons can be clearly seen.
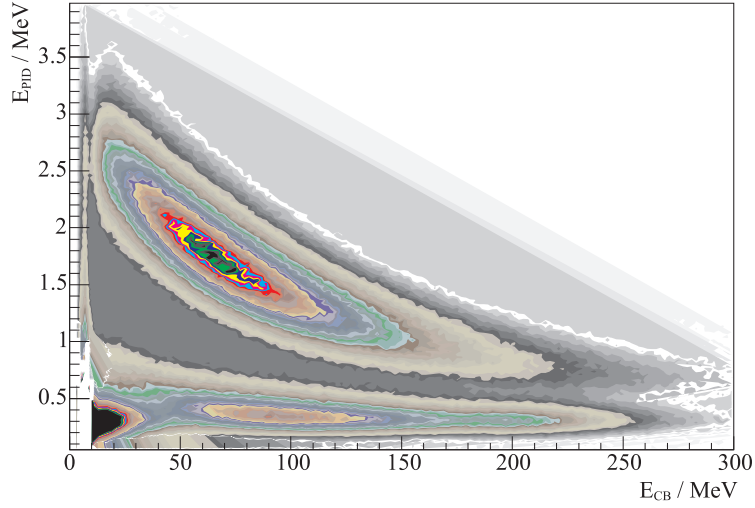

Figure 21: A typical $\Delta E/E$ plot from the Crystal Ball and the PID2 detector. The upper curved region is the proton locus, the lower region contains the pions and the peak towards the origin contains mostly electrons.

runs [43]. The most significant difference is that all detector signals are taken at the upstream end of the MWPCs, minimising the material required and facilitating particle detection in the forward polar region.

A mixture of argon (79.5%), ethane (30%) and freon-CF_4 (0.5%) is used as the filling gas. This mixture is a compromise between charge multiplication and localization requirements imposed by the ionizing particle tracks.

Within each chamber both the azimuthal and the longitudinal coordinates of the avalanche will be evaluated from the centroid of the charge distribution induced on the cathode strips. The location of the hit wires(s) will be used to resolve ambiguities which arise from the fact that each pair of inner and outer strip cross each other twice. The expected angular resolution (rms) will be $\sim 2°$ in the polar emission angle θ and $\sim 3°$ in the azimuthal emission angle ϕ.

The MWPCs have been recently installed inside the CB frame and their calibration using both cosmic rays and test beam data is currently underway.

3.4 TAPS Forward Wall

The TAPS forward wall is composed of 384 BaF$_2$ elements, each 25 cm in length (12 radiation lengths) and hexagonal in cross section, with a diameter of 59 mm. The front of every TAPS element is covered by a 5 mm thick plastic veto scintillator. The single counter time resolution is $\sigma_t = 0.2$ ns, the energy resolution can be described by $\Delta E/E = 0.018 + 0.008/E[GeV]^{0.5}$ [41]. The angular resolution in the polar angle is better than 1°, and in the azimuthal angle it improves with increasing θ, being always better than $1/R$ radian, where R is the distance in centimeters from the central point of the TAPS wall surface to the point on the surface where the particle trajectory meets the detector. The TAPS readout was custom built for the beginning of the CB@MAMI program and is effected in such a way as to allow particle identification by Pulse Shape Analysis (PSA), Time Of Flight (TOF) and $\Delta E/E$ methods (using the energy deposit in the plastic scintillator to give ΔE). TAPS can also contribute to the CB multiplicity trigger and is currrently divided into upto six sectors for this purpose. The 2 inner rings of 18 BaF$_2$ elements have been replaced recently by 72 PbWO$_4$ crystals each 20 cm in length (22 radiation lengths). The higher granularity improves the rate capability as well as the angular resolution. The crystals are operated at room temperature. The energy resolution for photons is similar to BaF$_2$ under these conditions [46].

4 Appendix B: simulated sensitivity of the experiment

In this appendix the results from the simulation of the sensitivity of the experiments for 700 h beam time with the longitudinally polarized target and 700 h beam time with the transversely polarized target are given. For the observables E, F, T the expected results for quasi-free protons and neutrons have been calculated assuming either the predictions of the full MAID model or the truncated model without contribution from the $D_{15}(1675)$ resonance. Results are given from threshold to the maximum incident photon energy in bins of 20 MeV.

- **detection efficincy for $\gamma d \rightarrow (n)p\eta$**
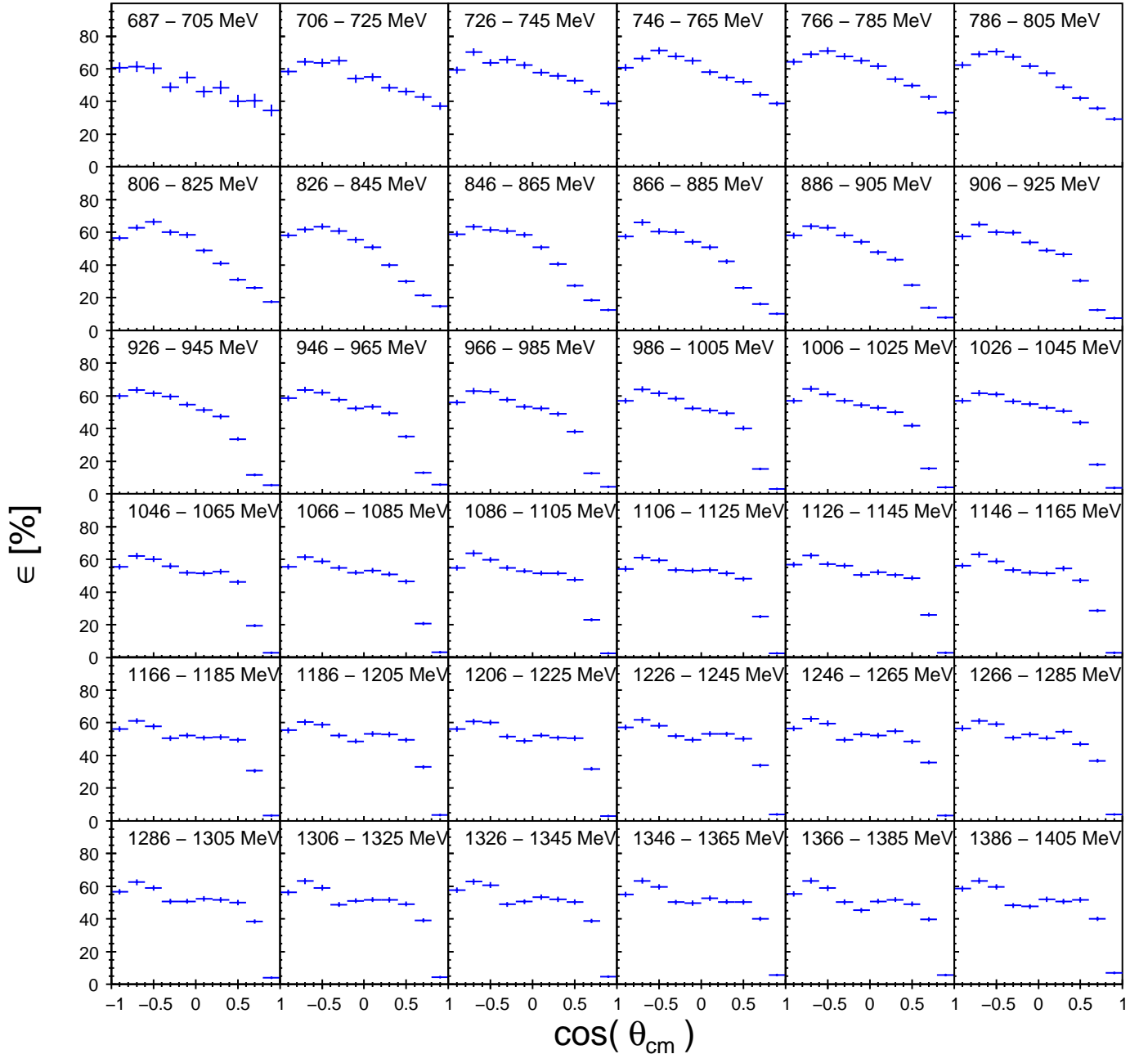
Figure 22: Simulated detection efficiency for quasi-free η-production of the proton

- **detection efficincy for** $\gamma d \to p(n)\eta$
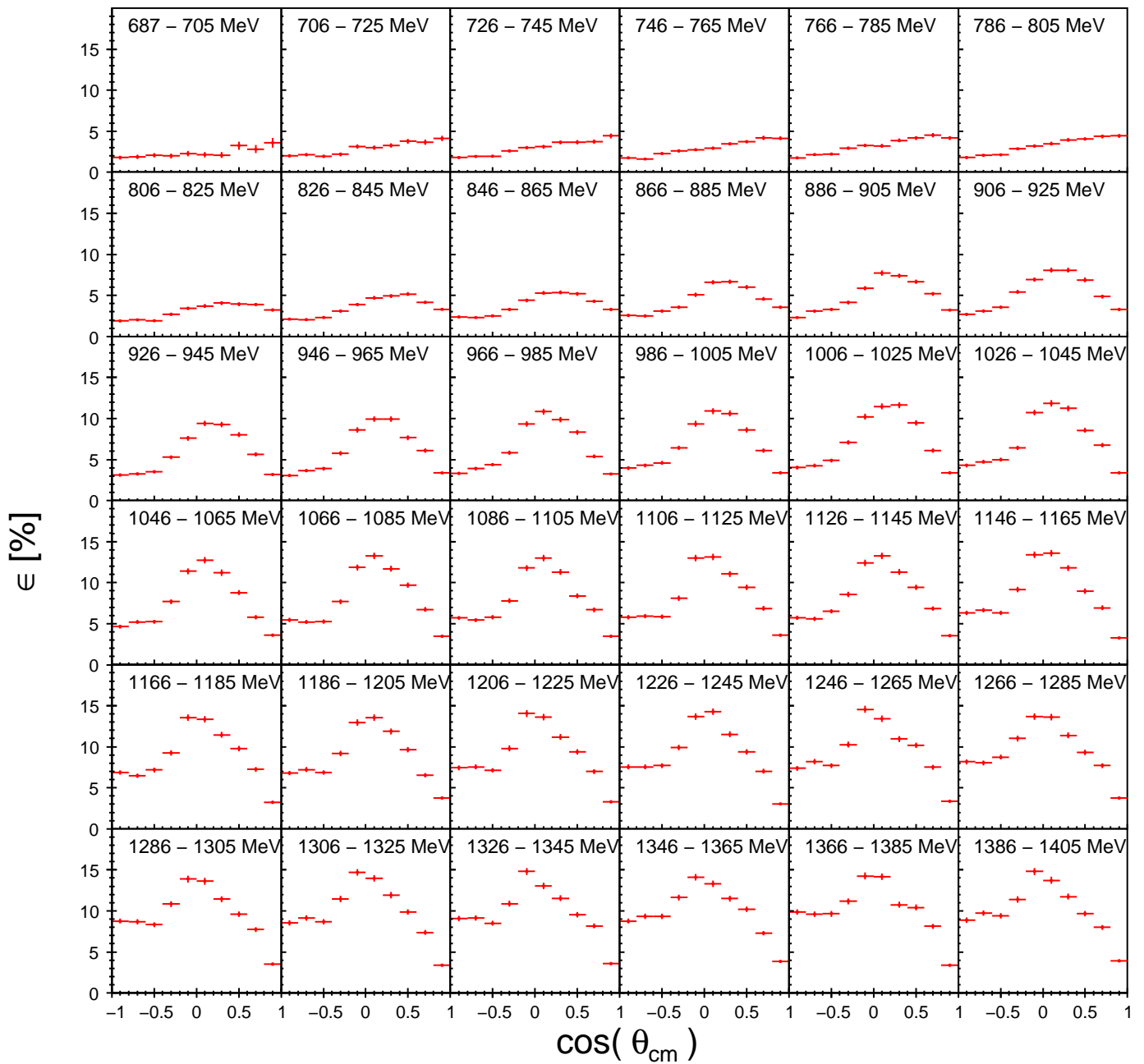
Figure 23: Simulated detection efficiency for quasi-free η-production of the neutron
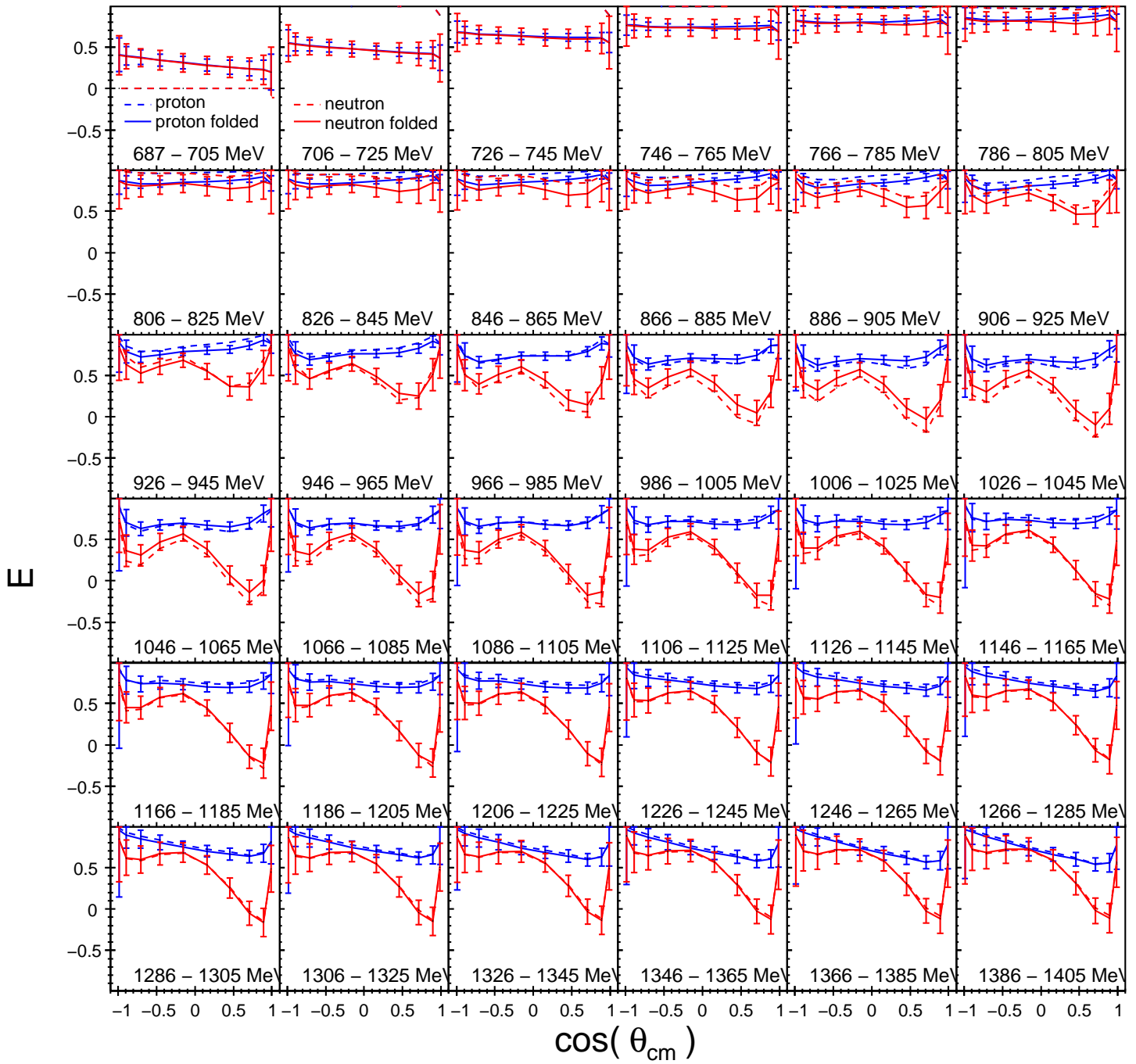
I) Observable E, full MAID model

Figure 24: Polarization observable E from full MAID-model. Blue: quasi-free proton, red: quasi-free neutron. Curves: solid prediction MAID model, dashed: folded with Fermi smearing, error bars: expected experimental precision
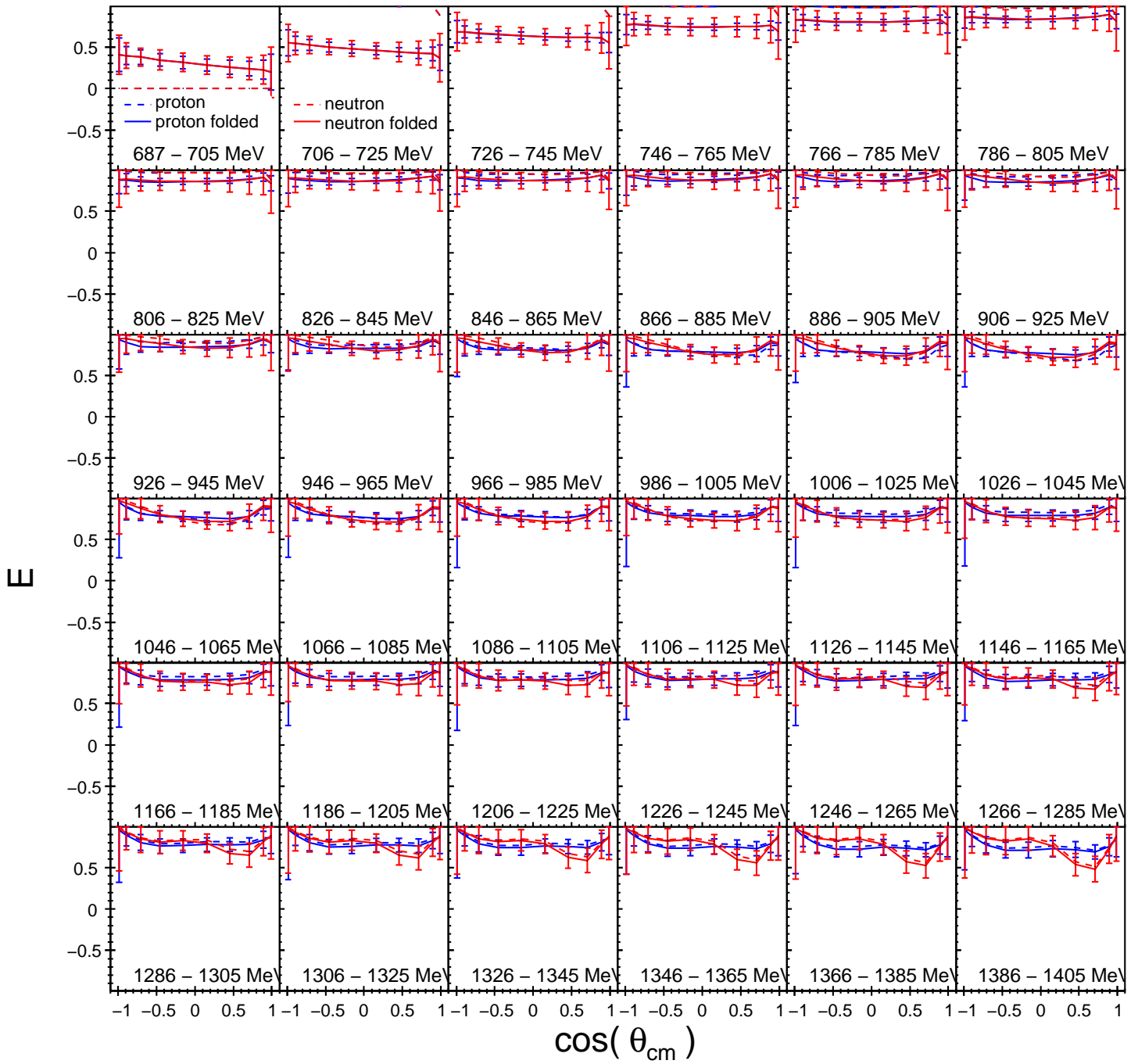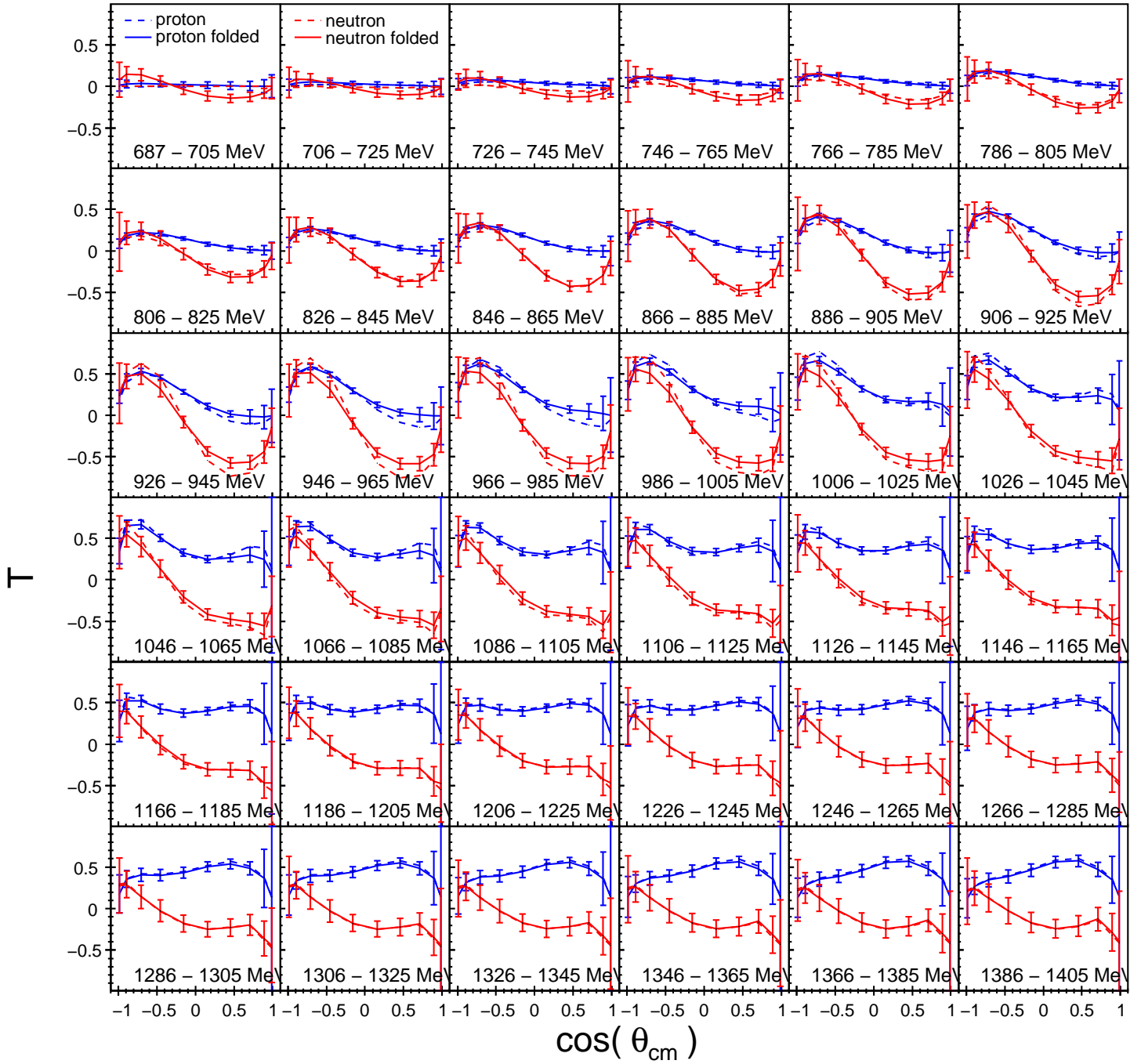
II) Observable E, MAID model without $D_{15}(1675)$

Figure 25: Polarization observable E from truncated MAID-model ($noD_{15}(1675)$). Blue: quasi-free proton, red: quasi-free neutron. Curves: solid prediction MAID model, dashed: folded with Fermi smearing, error bars: expected experimental precision

II) Observable T, full MAID model

Figure 26: Polarization observable T from full MAID-model (noD$_{15}$(1675). Blue: quasi-free proton, red: quasi-free neutron. Curves: solid prediction MAID model, dashed: folded with Fermi smearing, error bars: expected experimental precision
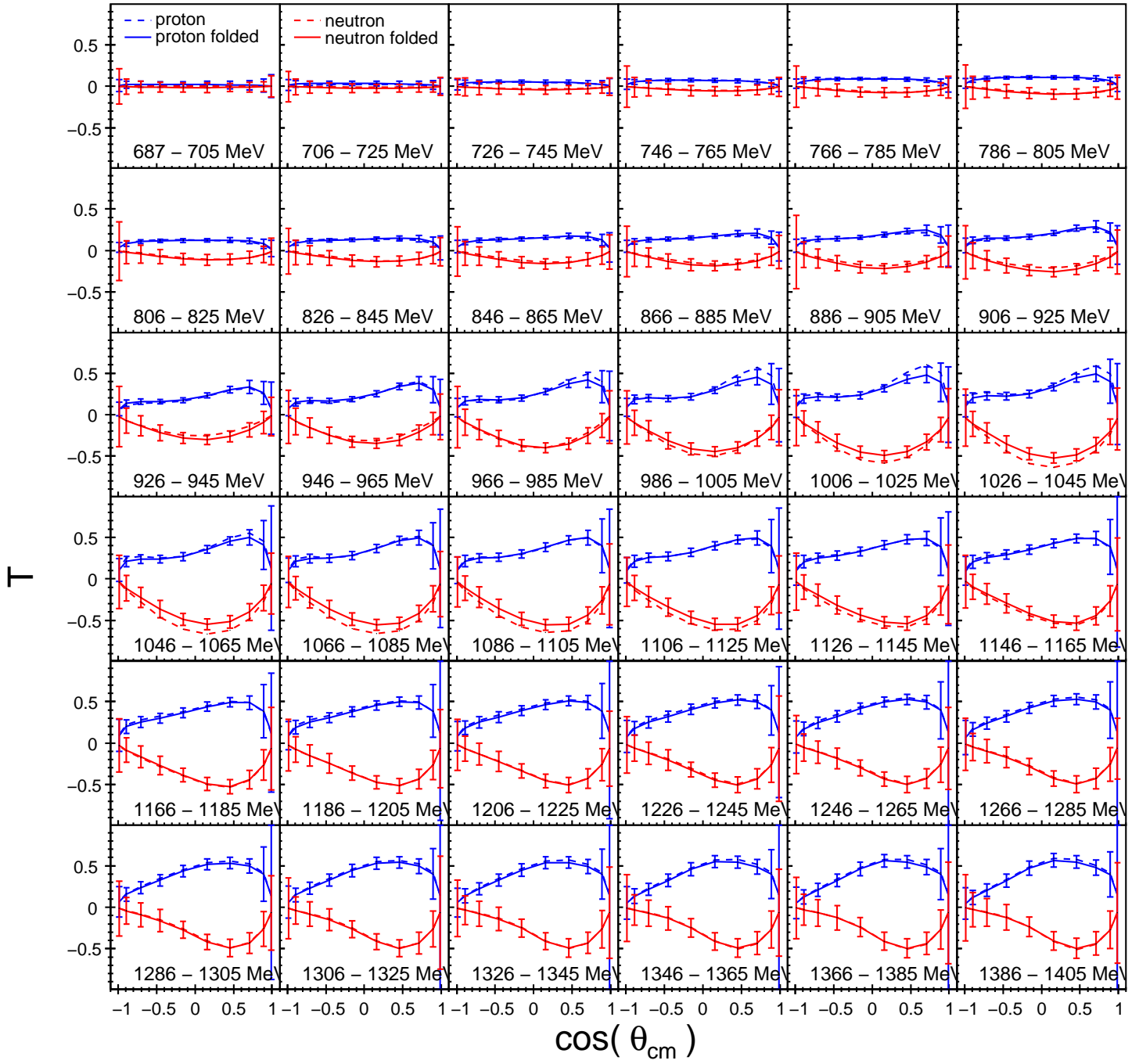
IV) Observable T, MAID model without $D_{15}(1675)$

Figure 27: Polarization observable T from truncated MAID-model (no$D_{15}(1675)$). Blue: quasi-free proton, red: quasi-free neutron. Curves: solid prediction MAID model, dashed: folded with Fermi smearing, error bars: expected experimental precision
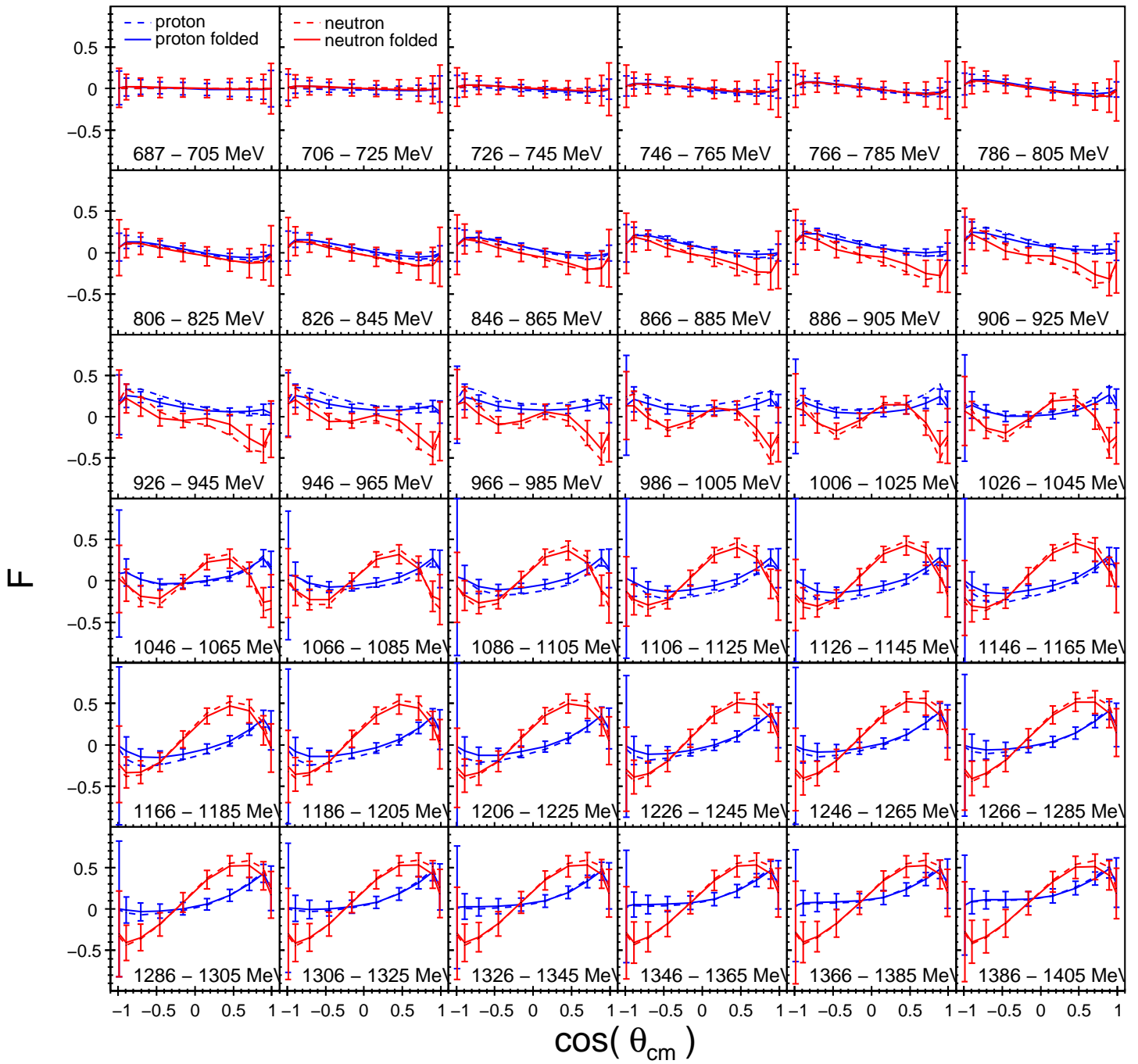
V) Observable F, full MAID model

Figure 28: Polarization observable F from full MAID-model (noD$_{15}$(1675). Blue: quasi-free proton, red: quasi-free neutron. Curves: solid prediction MAID model, dashed: folded with Fermi smearing, error bars: expected experimental precision
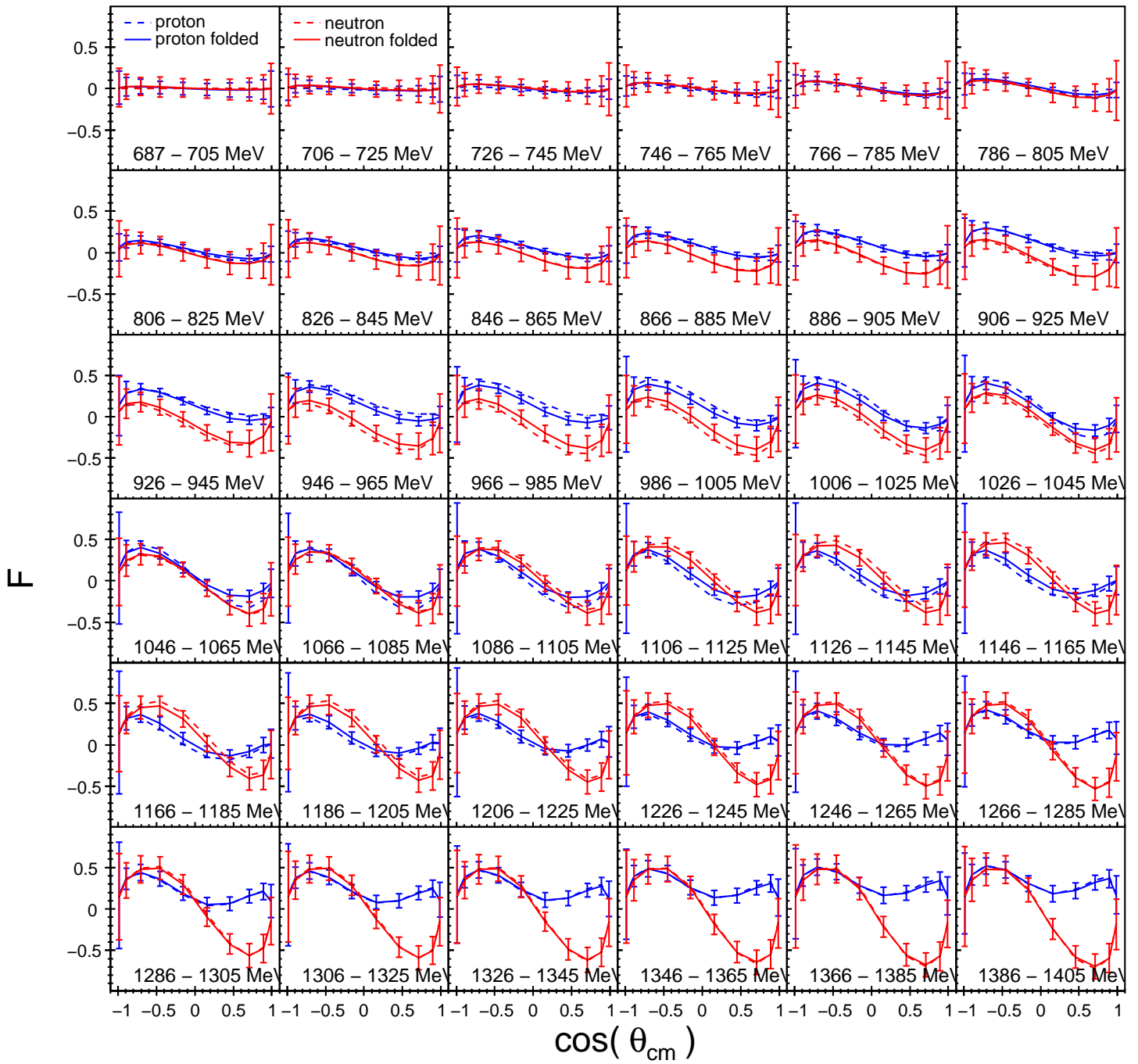
VI) Observable F, MAID model without $D_{15}(1675)$

Figure 29: Polarization observable F from truncated MAID-model (no$D_{15}(1675)$). Blue: quasi-free proton, red: quasi-free neutron. Curves: solid prediction MAID model, dashed: folded with Fermi smearing, error bars: expected experimental precision

References

[1] T. Burch et al., Phys. Rev. **D74** (2006) 014504.

[2] S. Capstick and W. Roberts, Prog. Part. Nucl. Phys. **45** (2000) 241.

[3] V.D. Burkert and T.-S. Lee, Int. J. Mod. Phys. **E13** (2004) 1035.

[4] B. Krusche and S. Schadmand, Prog. Part. Nucl. Phys. **51** (2003) 399

[5] B. Krusche et al., Eur. Phys. J. **A6** (1999) 309

[6] E.M. Darwish, H. Arenhövel, M. Schwamb, Eur. Phys. J. **A16** (2003) 111

[7] A. Sibirtsev et al., Phys.Rev **C65** (2002) 044007, 067002.

[8] B. Krusche et al., Phys. Lett. **B358** (1995) 40

[9] I. Jaegle et al., Phys. Rev. Lett. 100 (2008) 252002.

[10] P. Hoffmann-Rothe et al., Phys. Rev. Lett. **78** (1997) 4697

[11] V. Hejny et al., Eur. Phys. J. **A6** (1999) 83

[12] J. Weiss et al., Eur. Phys. J. **A11** (2001) 371

[13] V. Hejny et al., Eur. Phys. J. **A13** (2002) 493

[14] J. Weiss et al., Eur. Phys. J. **A16** (2003) 275

[15] M. Pfeiffer et al., Phys. Rev. Lett. **92** (2004) 252001

[16] N. Kaiser, P.B. Siegel, W. Weise, Phys.Lett. **B362** (1995) 23

[17] N. Kaiser, T. Waas, W. Weise, Nucl. Phys. **A612** (1997) 297

[18] D. Elsner et al., Eur. Phys. J. **A33** (2007) 147

[19] W.-T. Chiang, S.N. Yang, L. Tiator, D. Drechsel, Nucl. Phys. **A700** (2002) 429

[20] V.A. Anisovich et al., Eur. Phys. J **A25** (2005) 427.

[21] S. Eidelmann et al., Phys. Lett. B 592 (2004) 1

[22] V. Burkert et al., Phys. Rev. **C67** (2003) 035205

[23] V. Crede et al., Phys. Rev. Lett. **94** (2005) 012004

[24] R.A. Arndt, Ya.I. Azimov, M. Polyakov, I.I. Strakovsky, and R.L. Workman, Phys Rev **C69** (2004) 035208 Z. Phys. **A359** (1997) 305

[25] M. Polyakov and A. Rathke, Eur. Phys. J. **A18** (2003) 691

[26] H.C. Kim, M. Polyakov, M. Praszalowicz, G.S. Yang, K. Goeke, (2005) hep-ph/0503237

[27] D.K. Hong, (2004) hep-ph/0412132

[28] V. Kuznetsov et al., Proceedings of the NSTAR2004 workshop on Excited Nucleons, March 2004, Grenoble, France; hep-ex/0409032

[29] V. Kuznetsov et al., Phys. Lett. **B647** (2007) 23

[30] R.A. Arndt, W.J. Briscoe, I.I. Strakovsky, and R.L. Workman, http://gwdac.phys.gwu.edu

[31] V. Shklyar et al., Phys. Lett. **B650** (2007) 172.

[32] B. Krusche et al, Phys. Rev. Lett. **74** (1995) 3736.

[33] H. Denizli et al, Phys. Rev. **C76** (2007) 015204.

[34] O. Bartholomy et al., Eur. Phys. J **A33** (2007) 133.

[35] A. Fix et al., Eur. Phys. J. **A32** (2007) (2007)

[36] V.A. Anisovich et al., Eur. Phys. J. **A**, in press

[37] F. Miyahara et al., Prog. Theor. Physics Supplement 168 (2007) 90.

[38] D. Werthmueller, priv. com.

[39] I.S. Barker, A. Donnachie, J.K. Storrow, Nucl. Phys. **B95** (1975) 347.

[40] A. Fantini et al., Phys. Rev. **C78** (2008) 015203.

[41] S. Prakhov et al., Phys. Rev. **C79** (2009) 035204

[42] J.C. McGeorge et al., Eur. Phys. J. bf A37 (2008) 129

[43] G. Audit et al., Nucl. Instr. Meth. **A301** (1991) 473

[44] A. Reiter et al., Eur. Phys. J. **A30** (2006) 461

[45] A. Thomas et al., Nucl. Phys. **B79** (1999) 591

[46] R. Novotny et al.: Nucl. Instrum. Meth. **A486** (2002) 131